The basal interstitial nucleus (BIN) of the cerebellum provides diffuse ascending inhibitory input to the floccular granule cell layer

The basal interstitial nucleus (BIN) of the cerebellum provides diffuse ascending inhibitory input to the floccular granule cell layer

Journal:	*Journal of Comparative Neurology*
Manuscript ID	JCN-18-0028.R1
Wiley - Manuscript type:	Research Article
Keywords:	vestibulocerebellum, flocculus, GABA, Choline Acetyltransferase, Necab1, Golgi cells, gigantocellular reticular formation, human, macaque

Title: The basal interstitial nucleus (BIN) of the cerebellum provides diffuse ascending inhibitory input to the floccular granule cell layer

Running title: a novel inhibitory cerebellar neuron

Dick Jaarsma[1]*, Francois Blot[1], Bin Wu[1], Subramanian Venkatesan [1], Jan Voogd[1], Dies Meijer[2], Tom J.H. Ruigrok[1], Zhenyu Gao[1], Martijn Schonewille[1], and Chris I. De Zeeuw[1,3]

1. Dept. of Neuroscience, Erasmus MC, Wytemaweg 80, 3015 CN, Rotterdam, The Netherlands
2. Centre of neuroregeneration, University of Edinburgh, Edinburgh, UK
3. Netherlands Institute for Neuroscience, Royal Netherlands Academy of Arts & Sciences, Meibergdreef 47, 1105 BA, Amsterdam, The Netherlands

*** Correspondence**
Dr. Dick Jaarsma
Department of Neuroscience, Erasmus MC
Wytemaweg 80
3015 CN Rotterdam
d.jaarsma@erasmusmc.nl

Conflict of Interest: The authors declare no competing financial interests

Acknowledgements: This work was supported by the Dutch Organization for Life Sciences (NWO-ALW), Dutch Organization for Medical Sciences (Zon-MW), European Research Council (ERC-PoC; ERC-Starter). We are grateful to Elise D. Haasdijk for histological work; Gert-Jan Kleinrensink (Dept. of Neuroscience, ErasmusMC) for providing human cerebellar tissue; Rory de Vries, Judith van den Brand and Lineke Begeman (Viroscience, ErasmusMC) for macaque and ferret cerebellar tissue. Gert van Cappellen (Erasmus Optical Imaging Centre) for Fiji Macro scripts for confocal image analysis.

Author contributions: DJ, designed research and wrote the paper; DJ, FB, BW, TJHR, MS and ZG performed research; MS, DM, JV, TJHR, CIdZ contributed unpublished reagents/analytic tools; DJ, FB, ZG, SV analyzed data; CIdZ edited the paper.

Abstract

The basal interstitial nucleus (BIN) in the white matter of the vestibulocerebellum has been defined more than three decades ago, but has since been largely ignored. It is still unclear which neurotransmitters are being used by BIN neurons, how these neurons are connected to the rest of the brain and what their activity patterns look like. Here, we studied BIN neurons in a range of mammals, including macaque, human, rat, mouse, rabbit and ferret, using tracing, immunohistological and electrophysiological approaches. We show that BIN neurons are GABAergic and glycinergic, that in primates they also express the marker for cholinergic neurons choline acetyl transferase (ChAT), that they project with beaded fibers to the glomeruli in the granular layer of the ipsilateral floccular complex, and that they are driven by excitation from the ipsilateral and contralateral medio-dorsal medullary gigantocellular reticular formation. Systematic analysis of co-distribution of the inhibitory synapse marker VIAAT, labeled BIN axons and Golgi cell marker mGluR2 indicate that BIN axon terminals complement Golgi cell axon terminals in glomeruli, accounting for a considerable proportion (> 20%) of the inhibitory terminals in the granule cell layer of the floccular complex. Together, these data show that BIN neurons represent a novel and relevant inhibitory input to the part of the vestibulocerebellum that controls compensatory and smooth pursuit eye movements.

Keywords: vestibulocerebellum, flocculus, GABA, Choline Acetyltransferase, Necab1, Golgi cells, gigantocellular reticular formation, human, macaque, RRID: AB_2313712, RRID: AB_10000340, RRID: AB_10000320, RRID: AB_2313637, RRID: AB_11214092, RRID: AB_477652, RRID: AB_90715, RRID: AB_2278725, RRID: AB_303395, RRID: AB_302021, RRID: AB_94952, RRID: AB_1848014, RRID: AB2298772, AB5620; RRID: AB_91937, RRID: AB_887873, RRID: AB_887869, RRID: AB_2301751, RRID: AB_2315546, RRID: AB_1587626, RRID: AB_2187552, RRID: AB_2187539, RRID: AB_2307337

1. INTRODUCTION

The cerebellar cortex is well known for its relatively simple stereotyped trilaminar histo-architecture and sagittally organized modules (Voogd and Glickstein, 1998; Cerminara et al., 2015), and represents a powerful model system for investigating the organization and computations of complex central nervous system circuitries (Dean et al., 2010; De Zeeuw et al., 2011; Gao et al., 2012). The cerebellar cortex receives two main types of excitatory afferent systems, the climbing fiber system and the mossy-parallel fiber system, that converge on a single output neuron, the Purkinje cell that in turn provides inhibitory control of the cerebellar and vestibular nuclei. Climbing fibers arise from the inferior olive and innervate about 8-15 Purkinje cells each, providing an exceptionally strong direct synaptic connection with well over ~1,000 release sites distributed over a large portion of the dendritic tree (Palay and Chan-Palay, 1974; Davie et al., 2008; Gao et al., 2012). Mossy fibers originate from various sources in the brainstem and spinal cord and modulate Purkinje cell activity indirectly via the granule cells and inhibitory interneurons (Jelitai et al., 2016). With about 100-200 rosettes per mossy fiber, each innervating about 10-20 granule cells that in turn may form synaptic terminals with more than 500 Purkinje cells, the mossy fibers represent a highly divergent system (Harvey and Napper, 1988; Jakab and Hamori, 1988; Rancz et al., 2007; Gao et al., 2012). One of the key questions regarding the cerebello-cortical circuitry is how mossy fiber activity is translated into granule cell activity and subsequently integrated into Purkinje cell activity (Powell et al., 2015; Valera et al., 2016; Sudhakar et al., 2017).

Mossy fibers are morphologically heterogeneous, encode diverse modalities and may evoke greatly distinct patterns of excitatory responses in granule cells across different parts of the cerebellar cortex (Arenz et al., 2009; Huang et al., 2013; Chabrol et al., 2015; Gao et al., 2016). Therefore, it is feasible that also the down-stream cerebellar cortical circuitries display modality and task-depending variabilities (Arenz et al., 2009; Witter and De Zeeuw, 2015; Valera et al., 2016). For example, the activity patterns and learning mechanisms of different cerebellar modules may be dominated by Purkinje cells with different intrinsic electrophysiological and biochemical properties (Zhou et al., 2014; Cerminara et al., 2015; De Zeeuw and Ten Brinke, 2015). In addition, the flocculus and nodulus of the vestibulocerebellum, which are involved in compensatory eye and body movements (Ito, 1982; Schonewille et al., 2006; Lisberger, 2009; Voogd et al., 2012) show a marked enrichment of unipolar brush cells (UBCs), an excitatory granular layer interneuron, which can prolong the excitatory drive of the mossy fiber system (Gao et al., 2012; Sekerkova et al., 2014; van Dorp and De Zeeuw, 2015; Zampini et al., 2016). Furthermore, there is evidence for heterogeneity of inhibitory granule cell layer interneurons across distinct lobules (Neki et al., 1996; Simat et al., 2007; Ankri et al., 2015; Eyre and Nusser, 2016).

In the present study, we show that the granule cell layer of the flocculus receives an inhibitory input from a hitherto largely neglected population of neurons, the basal interstitial nucleus (BIN), which was originally identified by Langer in macaque (Langer et al., 1985; Langer, 1985). We found that BIN cells in human, rodents, ferret and rabbit are, just like in macaque, mainly located in the white matter of the lateral vestibulocerebellum, and that they are GABAergic and glycinergic. In addition, we show in rodents that BIN neurons receive a relevant and unique excitatory input from the medio-rostral medullary reticular formation. Our data indicate that the BIN represents a novel inhibitory afferent system, which may play an essential role in the proper conversion of mossy fiber activity into Purkinje cell firing in the flocculus.

2. MATERIALS AND METHODS

2.1 Animals

Mutant mouse models, primary antibodies and other key resources are summarized in Table 1. All animal experiments were performed in accordance with the guidelines the Dutch national and European legislation and were approved by the animal welfare committee for animal experiments of the Erasmus Medical Center. Male and female C57BL/6 mice, aged 2- 6 months of age, were obtained from the ErasmusMC animal core facility. BALB/c mice were from Charles River. GlyT2GFP transgenic mice (Table 1) that express enhanced green fluorescent protein under the control of the glycine transporter type 2 promoter were kindly provided by Dr. Fritschy (Zeilhofer et al., 2005) and maintained as hemizygotes in C57BL/6 background in the ErasmusMC animal core facility. VGluT2-ires-Cre knock-in mice, generated by Dr. Lowell (Vong et al., 2011), were obtained from Jackson Laboratories (JAX#016963, Table 1), and maintained as homozygotes in the Erasmus MC animal core facility. Young (3-4 weeks) and adult (3-6 months) male Wistar rats were obtained from Charles River. Animals were group housed until surgery, fed ad libitum, and kept at 12:12 light/dark cycle. Cerebella from adult pigmented Dutch belted rabbits (n = 2), ferret (n = 2), and macaque monkey (n = 4) were derived from animals used in other studies (Jaarsma et al., 1995; Ruigrok et al., 2011; van Riel et al., 2013; Siegers et al., 2014).

2.2 Human tissue. Human cerebella were obtained via the Dutch National body donation program. Donors gave their informed and written consent to the donation of their bodies to the Erasmus MC for research and education purposes. In this study we used cerebellar tissue from two male donors who died at 74 and 78 years of age. Cerebellar specimens were dissected within 48 h following death and fixed in formalin for 6-8 weeks.

2.3 Stereotaxic injections

For stereotaxic injections of Cholera toxin B-subunit (CTB) in rat flocculus, animals (n = 2) were anesthetized with an intraperitoneal injection of thiazinehydrochloride (3 mg/kg) and ketamine (100 mg/kg), placed in a stereotactic frame, and their caudal vermis was exposed by removing overlying skin and neck muscles and opening of the atlanto-occipital membrane and dura. Carprofen (Rimadyl Cattle i.p. 5 mg/kg) and lidocaine (s.c. 0,4 mg/ml) were used to reduce perisurgical pain. The flocculus was approached by a glass micropipette (tip diameter 10 - 20 µm), placed horizontally at an angle of 50 degrees with the rostrocaudal axis, and penetrating the cerebellum 6.5 mm starting from the midline at the border of lobule IX-B and -C (Ruigrok, 2003). 100 nl CTB (1% w/v in phosphate buffered saline, pH 7.2, 0.1 M) was injected with mechanical pressure at a speed of 10 nl/min. After

injection, the pipette was left in place for >10 minutes before being slowly withdrawn. After a survival period of 5 to 7 days, rats were deeply anesthetized with an overdose of Nembutal (200 mg/kg) and transcardially perfused with an initial flush of 500 ml 0.9% saline, followed by 1 liter of 4% paraformaldehyde (PFA) in 0.12 M phosphate buffer (PB, pH 7.4).

Methods for stereotaxic injections in mice were largely as previously reported (Schonewille et al., 2006; Boele et al., 2013; Gao et al., 2016). During surgery mice were anesthetized with a mixture of isoflurane/oxygen (5% for induction, 1.5-2.0% for maintenance), while carprofen (Rimadyl Cattle i.p. 5 mg/kg), buprenorphine (Temgesic, i.p. 0.05 mg/kg), lidocaine (s.c. 0,4 mg/ml) and bupivacaïne (s.c. 0,1 mg/ml) were applied to reduce perisurgical pain. Ophthalmic ointment was applied to the eyes to prevent corneal drying and damage. Body temperature was monitored and kept constant at 37°C throughout the entire surgical procedure. Mice were positioned on a custom-made mouse stereotaxic head-holding frame following the Paxinos mouse brain atlas (Paxinos and Franklin, 2001), small craniotomies (diameter ~3 mm) were made in corresponding sites, and injections were performed using glass pipettes (tip opening 8 - 15 µm) with mechanical pressure or iontophoresis. After each injection, the pipette was left in place for >10 minutes before being slowly withdrawn. For retrograde tracing, 40-100 nl of CTB (1% w/v in phosphate buffered saline, pH 7.2) was injected with mechanical pressure (speed 10 nl/min). For anterograde tracing biotinylated dextran amine 10 kDa (BDA, 10% w/v in saline, ThermoFisher) was applied with mechanical pressure (20-100 nl) or iontophoresis (pulses of 4 µA, 10 min). Alternatively, anterograde tracing was performed using AAV viral vector expressing enhanced GFP (Harris et al., 2012; Wang et al., 2014): 50-100 nl purified AAV1.CAG.CI.eGFP.WPRE.rBG (AAV-GFP, 10^{12}-10^{13} GC/ml) or AAV1.CAG.Flex.eGFP.WPRE.bGH (AAV-Flex-GFP), purchased from UPenn Vector Core (Table 1, https://pennvectorcore.med.upenn.edu/gtp/default.php), were pressure injected. To examine BIN axons in the flocculus, AAV-GFP was injected in C57BL/6 mice (n=10) using the following coordinates: 1.4 posterior of Lambda, 2.4 mm lateral and 2.6 mm ventral of the pial surface. The same coordinates were used for CTB injections in the BIN of C57BL/6 mice (n=4) to characterize brain stem neurons that innervate BIN neurons. This retrograde approach was complemented by an anterograde tracing approach with BDA injections made throughout the medulla oblongata and the pontine reticular formation of C57BL/6 mice (n=20). Coordinates of BDA injections in the medullary gigantocellular reticular nucleus that resulted in labeling of fibers innervating BIN neurons were 2,3-2,6 mm posterior of lambda, 0,2-0,4 mm lateral, 4,6 - 4,8 ventral of the pial surface. These coordinates were also used for AAV-Flex-GFP injections in VGluT2-Cre mice (n=2) to demonstrate that medullary gigantocellular reticular nucleus projections to BIN neurons were VGluT2+ neurons. For a subset of BDA injections (n = 15 mice) the squamosal part of the occipital bone was freed and the atlanto-occipital membrane and dura were opened, to approach the medulla oblongata from caudal with the pipette positioned at an angle of 45° in the rostro-caudal direction. For injection in the inferior

olive, penetrations were made with reference to the obex and guided by electrophysiological recording, and injections were made using iontophoresis (Ruigrok et al., 1992). Also injection in the medial vestibular prepositus hypoglossal nuclei were guided by electrophysiological recordings. CTB injections in the floccular cortex were performed in alert, head-fixed restrained GlyT2GFP (n=3) and C57BL/6 (n=2) mice placed on a platform in the center of a random dotted drum to enable identification of floccular zones on the basis of complex spike modulation of Purkinje cells triggered by optokinetic stimulation (Schonewille et al., 2006). In these mice, a head fixation pedestal was fixed to the skull with dental cement (Charisma, Heraeus Kulzer, NY, USA) 5 days prior to injection, and a recording chamber was made following craniotomy of the occipital bone (Schonewille et al., 2006).

Post-injection survival times for injected mice were 5-8 days (CTB, BDA) or 2-3 weeks (AAV). Mice were deeply anesthetized with an overdose of Nembutal (i.p. 200 mg/kg), transcardially perfused with 20 ml saline followed by 100 ml 4% PFA in 0.12 M PB, and brains were removed, post-fixed for 2 h in 4% PFA, and embedded in 12% gelatin further processed for histology.

2.4 Antibody characterization

Primary antibodies used for immunohistology were from commercial sources with the exception of a rat monoclonal antibody against Lgi2 (see Table 1 for Immunogen, source, catalogue number, RRID number, and final antibody concentration of each primary antibody). The commercial primary antibodies have been well characterized in previous studies (Jaarsma et al., 1995; Jaarsma et al., 1996; Singec et al., 2004; Simat et al., 2007; Gao et al., 2016; Zhang et al., 2016). Validation of labeling specificity in this study is based on the expected distribution pattern compared to these studies. The rat-anti Lgi2 antibody (clone Lgi2-10D6) was raised against a full length Lgi2-Fc fusion protein. Immunization of rats with antigen, and production of hybridoma cell lines was performed by Absea (http://www.absea-antibody.com). The labelling specificity for Lgi2 was determined using cerebellar sections from Lgi2 knockout mice, which did not show any labelling. Furthermore, the labelling pattern in the cerebellar cortex is consistent with the expected distribution based on mRNA expression in Allan Brain Atlas (Lein et al., 2007). Further details of the production and validation of the rat-anti Lgi2 antibody will be reported elsewhere.

2.5 Immunohistology

The following material was processed for immunohistology: brains from mouse and rat who received tracer injections; brains from additional transcardially 4% PFA perfused mice (n= 12; C57BL/6 or BALB/c), rats (n =4), rabbits (n=2) and macaque (n= 4), immersion (6-8 weeks) formalin-fixed brains from ferret (n=2), and formalin-fixed blocks from humans containing the flocculus, tonsils and deep nuclei. Brain samples were embedded in 11% gelatin (type B, JT Baker 2124, Fisher Scientific, CAS number: 9000-70-8), incubated overnight in 30% sucrose at 4 °C, and cut into 40 or

50 µm coronal sections on a sliding freezing microtome (Leica SM 2000R). Sections were serially collected in 8 (mouse, rat), 20 (ferret, rabbit, macaque) or 40 (human) vials with phosphate buffered saline (PBS, pH 7.2) such that each vial contained a complete series of sections. Sections were processed free-floating for diaminobenzidine (DAB, 0.05%)-immunoperoxidase histochemistry or immunofluorescence (Kuijpers et al., 2013). Following preincubation in PBS containing 0,4% Triton X-100 (PBST) and normal horse serum (NHS) and for 1 h at room temperature, sections were incubated 48-60 h at 4°C with the primary antibodies in PBST with 2% NHS. For immunoperoxidase histochemistry, sections were subsequently incubated with biotinylated secondary antibodies raised in donkey (diluted 1:400; Jackson, Burlingame, CA) for 2 h at room temperature, followed by incubation in avidin-biotin-immunoperoxidase complex (ABC; diluted 1:400; Vector Laboratories) and the reaction with DAB as described by the manufacturer. To visualize BDA in anterograde tracing experiments, sections following the preincubation step, were incubated with ABC and processed for DAB staining. Sections were mounted on glass-slides, air-dried, and counterstained with Thionin (1%) to outline cell nuclei and Nissl substance in neurons. Immunoperoxidase-stained sections were analyzed using a Leica (Nussloch, Germany) DM-RB microscope, or scanned with a Hamamatsu NanoZoomer 2 whole slide imager and analyzed with NDP.view (Hamamatsu) software. Immunoperoxidase histochemistry was performed with series of sections of BDA and CTB tracing experiments to examine injection area and map projection fibers and retrogradely labeled neurons, respectively. In addition, immunoperoxidase histochemistry was used for mapping BIN neurons using the following antibodies: goat anti-ChAT (1:500; Millipore AB144P, RRID:AB_11214092), rabbit anti-Glutamic acid decarboxylase 65 and 67 (GAD; 1:2000; Millipore AB1511, RRID:AB_90715), mouse anti-GAD67 (1:1000; Millipore MAB5406), rabbit anti-Necab1 (1:1000; Sigma, HPA023629; RRID:AB_1848014), or mouse anti-NeuN (1:2000; Millipore, MAB377; RRID:AB2298772).

For immunofluorescence, sections were incubated with multiple combinations of primary antibodies (see table 1), followed by incubation with fluorescently-labeled secondary antibodies raised in donkey, diluted 1:400 in PBST-2%NHS, and carrying Alexa Fluor 405 (A405), A488, Cy3-, or A647 as fluorophores (Jackson Immunoresearch or ThermoFisher). Typically, in triple labelling experiments A488, Cy3 and A647-labeled secondary antibodies were used, and section were counterstained with Dapi to visualize cell nuclei, while in quadruple labelling experiments A405-labeled secondary antibody was used, and Dapi was omitted. In sections from BDA tracing experiments, BDA was labeled with A488 streptavidin (ThermoFisher). Sections stained for immunofluorescence were mounted on coverslips, placed on glass slides with Vectashield mounting medium, and were examined with Zeiss LSM 510 and LSM700 confocal laser scanning microscopes.

2.6 Immuno-electron microscopy

Two mice receiving an AAV-GFP injection in the BIN were perfused with 100 ml 0.12 M PB buffered 4% PFA with 0.5% glutaraldehyde, and further processed for anti-GFP immuno-peroxidase DAB electron microscopy: the cerebellum was removed, post-fixed overnight in 4% PFA, and cut in 60 µm coronal sections on a vibratome. Sections were subjected to a freeze-thaw procedure to improve antibody penetration and incubated for 96 h at 4°C with rabbit-anti-GFP antibody (1:5000, Abcam) in Tris-buffered saline (TBS, pH7.4), followed by incubation with biotinylated-goat-anti-rabbit secondary antibody (1:200 in TBS, overnight at 4°C), and incubation with ABC (1:400 in TBS overnight at 4°C), and subsequent reaction with DAB. Subsequently, sections were rinsed and post-fixed in 1% osmium tetroxide, stained with 1% uranyl acetate, dehydrated and embedded in araldite (Durcupan ACM; Fluka, Buchs, Switzerland). Semi-thin (500 nm) and ultrathin (50-70 nm) sections were cut on an ultramicrotome (Leica, Wetzlar, Germany). Semi-thin were mounted on glass slides and stained with toluidine blue and analyzed light-microscopically. Ultrathin sections were mounted on formvar-coated grids, contrasted with 2% uranyl acetate and 1% lead citrate (Fluka), and examined using a Phillips CM100 electron microscope at 80 kV (Philips, Eindhoven, Netherlands). A subset of grids were processed for GABA immunogold labelling. The grids were rinsed in TBS with 0.1% Triton X-100, pH 7.6 (TBST), and incubated overnight at 4ºC with rabbit anti-GABA (Sigma, 1:1500 in TBST) antibody. The grids were subsequently rinsed twice with TBST and incubated for 1 h at room temperature in goat anti-rabbit IgG labeled with 10 nm gold particles (Aurion) diluted 1:50 in TBST.

2.7 Slice recording

3-4 weeks old Wistar rats were decapitated under isoflurane anesthesia. 300 µm thick cerebellar coronal slices containing the flocculus were cut on a vibratome (VT1200s, Leica, Wetzlar, Germany) in icecold slicing medium containing (in mM): 240 Sucrose, 5 KCl, 1.25 Na2HPO4, 2 MgSO4, 1 CaCl2, 26 NaHCO3 and 10 D-Glucose, bubbled with 95% O2 and 5% CO2. Slices were incubated at 34°C for 1 h in the oxygenated ACSF containing (in mM): 124 NaCl, 2.5 KCl, 1.25 Na2HPO4, 1 MgSO4, 2 CaCl2, 26 NaHCO3 and 25 D-Glucose and kept at room temperature (21 ± 1 °C) before use. Experiments were performed with a constant flow of oxygenated ACSF (1.5-2.0 ml/min) at 34 ± 1 °C. Putative BIN neurons were identified under DIC visualization based on their distribution in the floccular white matter, and their relative large size compared to other white matter cells. Patch-clamp recordings were performed using an EPC-10 double amplifier controlled by the Patchmaster software (HEKA electronics, Lambrecht, Germany) (Gao et al., 2016). All recordings were low-pass filtered at 5 kHz and digitized at 20 kHz. Borosilicate glass pipettes (WPI) were filled with intracellular solution containing the following (in mM): 120 K-gluconate, 9 KCl, 10 KOH, 3.48 MgCl2, 4 NaCl, 10 HEPES, 4 Na2ATP, 0.4 Na3GTP and 17.5 sucrose (pH 7.25) and had pipette resistances of 3-5 MΩ. Spontaneous action potential firing of BIN neurons were recorded in loose

cell-attached mode prior to attaining the whole-cell configuration. After obtaining stable whole-cell configuration, a series of constant depolarizing current pulses with incremental amplitudes (20 pA/step) was applied to each cell to elicit voltage action potential firing patterns. For voltage clamp recordings of spontaneous EPSCs (sEPSCs), cells were recorded for >3 mins at -65 mV. At the end of the recording, a 5 mV hyperpolarizing voltage step was applied and the cell capacitance were calculated based on the decay of capacitive current.

For morphological characterization of recorded BIN neurons, neurobiotin (1% w/v) was added to the intracellular solution. After recording, slices were fixed in 4% PFA at room temperature for 2 h, washed in PBS overnight, and processed for immunofluorescence with guinea-pig anti VGluT1, mouse anti-mGluR2, and rabbit α-GAD as primary antibodies; A405 donkey anti-guinea-pig IgG, Cy3 donkey anti-mouse, and Cy5 donkey anti-rabbit as secondary antibodies; and A488 streptavidin (1:400, ThermoFisher) to visualize neurobiotin. Slices were carefully mounted in Vectashield and examined with LSM 700 confocal microscopes (Carl Zeiss, Jena, Germany). The slices were scanned at 0.5 x 0.5 x 2 µm (xyz) resolution using a Plan-Apochromat 20x (n.a. 0.8) objective and the tile function. The confocal stacks were used to trace the dendritic and axonal arborization of biocytin filled cells using Neurolucida software (MicroBrightField, Inc., Colchester, VT).

2.8 Analyses

To map and count BIN neurons in different species, series of sections processed for bright-field microscopy were examined and plotted using an Olympus microscope fitted with a Lucivid miniature monitor and Neurolucida software (MicroBrightField, Inc., Colchester, VT), while fluorescently-labeled section selected areas were scanned at a 0.625 x 0.625 x 2.5 µm (xyz) resolution using a LSM 700 confocal microscopes (Carl Zeiss, Jena, Germany) with Plan-Apochromat 20x (n.a. 0.8) objective and the tile function, and analyzed using ImageJ. To plot and count BIN neurons in macaque cerebellum we used 1 in 5 transverse thionin-stained serial sections (section thickness 40 µm, 160 µm interval between sections), and 1 in 10 GAD- and ChAT-immunoperoxidase stained series (360 µm between sections). Only cells with a visible nucleus were counted. In case of human cerebellum, ChAT-stained serial sections in a final frequency of 1 in 10 (section thickness 50 µm, 450 µm interval between section) were used for counting and plotting BIN neurons. For mapping the distribution of BIN neurons in rat, we used 1 in 4 CTB-immunoperoxidase/thionin stained series of transverse sections (120 µm interval) of previously documented (rat #798, rat #802, rat #836; Ruigrok, 2003) CTB experiments, and 1 in 4 CTB/GAD immunofluorescent stained series from 2 additional CTB tracing injections in rat flocculus (rat B1, rat B2). To estimate the relative size of the injection in each section, the ratio of the area of the injection occupying the floccular granule cell layer, and the area of the entire floccular granule cell layer were determined, and the means of these ratio's were calculated for each experiment. To count the total number of BIN neurons in rat cerebellum, additional

1 in 4 series stained for thionin, or GAD/NeuN immunofluorescence were used. For mapping and counting BIN neurons in mouse cerebellum, we used 1 in 4 series of transverse fluorescent sections (120 µm interval) labeled for CTB/GlyT2GFP (n = 3 mice) or CTB/Necab1 (n = 2 mice). For mapping and counting Golgi cells in the vermis 4-5 and the flocculus we used 1 in 4 series of transverse section from GlyT2GFP mice (n=4) stained for Lgi2/Necab1 or Lgi2/neurogranin.

For mapping and counting BIN neurons in ferret, we used 40 µm GAD-immunoperoxidase stained sections at frequencies of 1 in 5 (160 µm interval). For mapping BIN neurons in rabbit, we used previously documented WGA-HRP experiments with tracer injections in the floccular cortex (K227, K244, K358, K360; Tan et al., 1995) and 40 µm GAD-immunoperoxidase stained sections at frequencies of 1 in 10 (360 µm interval between sections).

To analyze anterograde BDA tracing experiments with injections made throughout the brainstem, 1 in 4 sections were processed for ABC peroxidase-DAB staining to map the injection area, and examine the floccular white matter for the presence of BDA+ beaded fibers contacting BIN neurons. In case of the presence of BDA+ beaded fibers, adjacent series of sections were processed for triple labeling fluorescence to outline BDA+ fibers (visualized with A488 streptavidin), VGluT2+ excitatory synaptic boutons, and BIN neurons (with either anti-Muscarinic M2 or anti-Necab1 antibodies). BIN neurons were examined for the presence of BDA+VGluT2+ and BDA-VGluT2+ boutons using a LSM 700 confocal microscope with Plan-Apochromat 40x (n.a. 1.3) and 63x (n.a. 1.4) oil objectives. Only BDA+VGluT2+ and BDA-VGluT2+ boutons contacting BIN cell bodies and their proximal dendrites were analyzed.

To examine the proportion of VIAAT+ axon terminals in macaque flocculus and dorsal paraflocculus that where either ChAT+ or mGluR2+, Z-stacks of 20 x 20 x 10 µm (12 optical sections of 1,5 µm thickness) of glomeruli were collected from ChAT/VIAAT/mGluR2 stained sections using an 63x oil objective. Glomeruli were identified on the basis of a grossly circular arrangement of VIAAT+ boutons (e.g. Fig. 2g,h). A contour was drawn around the glomerular profile and VIAAT+ boutons within the contour were examined for the presence of ChAT and mGluR2 signal. To estimate the proportion of VIAAT+ axon terminals in mouse cerebellar lobules that where mGluR2+, Z-stacks of 100 x 100 x 3 µm (3 optical sections of 1,5 µm thickness) of granule cell layer 2 µm below the surface of the section were collected from GFP/VIAAT/mGluR2 triple labeled sections using the 63x oil objective. Stacks were made in lobule III of the anterior vermis, the nodulus and the flocculus of a mice showing high levels of BIN axonal labelling in the flocculus following AAV-GFP injections in the BIN (VBIN2, VBIN3, VBIN5). VIAAT, GFP and mGluR2 signals were converted to binary images using the 'internodes' thresholding function in imageJ, and the area showing VIAAT labeling, as well as showing either VIAAT-mGluR2 or VIAAT- GFP double-labeling were determined per Z-stack (= means of 3 optical sections).

2.9 Allen mouse brain atlas

We screened the Allen Mouse Brain Atlas (Allen Institute for Brain Science, Seattle, WA; available from www.brain-map.org, (Lein et al., 2007)) for genes expressed in the mouse BIN using the AGEA (Anatomic Gene Expression Atlas) viewer modus of Allen Brain Atlas with 10400, 4800, 3000 as the seed voxel coordinates and 1.0 as the expression threshold. This modus enabled efficient visual inspection of nearly 2000 genes for expression in intermediate-large cells in the floccular white matter of the anterior flocculus. The method of screening was not exhaustive and was biased towards genes with relatively low expression in the granule cell layer, facilitating the detection of gene expression in the white matter. Genes with moderate to strong expression throughout the cerebellar white and grey matter, generally representing genes expressed by glia cells, were ignored.

2.10 Statistical analyses

Statistical analyzes were performed with Graphpad Prism using Student's t-test and ANOVA. Data are expressed as Means ± SE.

3. RESULTS

3.1 ChAT (choline acetyltransferase) immunostaining outlines the basal interstitial nucleus (BIN) in macaque cerebellum

While analyzing the distribution of immunoreactivity of choline acetyltransferase (ChAT, the terminal biosynthetic enzyme for acetylcholine) in macaque cerebellum, we identified a group of ChAT+ cells dispersed in the white matter ventrolateral of the cerebellar nuclei (Fig. 1a). The distribution and morphology of these ChAT+ neurons coincided with that of the basal interstitial nucleus (BIN), identified by Langer after retrograde tracing injections in the flocculus or the ventral paraflocculus (Langer et al., 1985; Langer, 1985). Like BIN neurons, ChAT+ cells had relatively large polymorphic cell bodies (area = 441 ± 18 μm^2, 251-720; mean ± SE, range, n=40 cells), and formed a cluster that extended from the hilus of the ventral paraflocculus to the white matter of the most rostral folium of the nodulus, respectively, with most ChAT+ cells in the white matter medial of the stalk of the flocculus (Fig. 1a,f). While most BIN neurons had a fusiform elongated morphology with dendrites emanating from each end, other BIN neurons showed pyramidal and polygonal morphologies (Fig. 1b). Notably, ChAT+ cells were also observed in Group Y, medial of the BIN, but these cells were much smaller (104 ± 5 μm^2, mean ± SE, n=10 cells) and clearly distinguishable from ChAT+ BIN cells (Fig. 1c).

In accord with the notion that BIN neurons innervate the flocculus/ventral paraflocculus (also referred to as the floccular complex; see Voogd et al., 2012), ChAT+ fibers in the BIN were oriented towards the white matter of the floccular complex, and a high density of ChAT+ fibers occurred in the white matter and granule cell layer of the floccular complex (Fig. 1a,d). In the granule cell layer, the ChAT+ fibers provided multiple beaded branches resulting in a dense plexus of ChAT+ varicose fibers (Figs 1d). These beaded ChAT+ fibers occurred throughout the floccular complex, but were absent in other cerebellar lobules, including the dorsal paraflocculus (Fig. 1e) and the nodulus. The density of ChAT+ fibers varied across different lobules of the floccular complex: grossly, ChAT+ fibers were more frequent in the flocculus than in the ventral paraflocculus and were denser in the basal than the apical part of individual folia (Fig.1f). Together, the data indicate that BIN neurons in macaque are ChAT+ and provide dense ChAT+ innervation of the granule cell layer in the floccular complex.

3.2 BIN neurons provide GABAergic input to the granule cell layer of the flocculus/ventral paraflocculus

Further characterization of the neurochemical identity of macaque BIN neurons showed that BIN neurons also stained positive with anti-glutamic acid decarboxylase (GAD) antibody. GAD/ChAT double labeling showed that all ChAT+ BIN neurons stained positive for GAD (Fig. 2a,

b), while an additional population of neurons inside the macaque BIN territory was negative for ChAT, but stained positive for GAD (Fig. 2a, b). These GAD+ChAT- BIN neurons showed the same size and morphologies as those of GAD+ChAT+ BIN neurons. Thus, the BIN in macaque may comprise 2 neurochemically distinct populations of neurons, GAD+ChAT+ and GAD+ChAT- neurons. Counting of serial ChAT and GAD immunoperoxidase stained sections indicated that there were about 1000 ($1.3 \pm 0.3 *10^3$, mean ± SE, n= 3) ChAT+ and 2000 ($2.2 \pm 0.2 *10^3$, n= 3) GAD+ BIN cells per half macaque cerebellum.

GAD/ChAT double labelling also showed that the cell bodies and proximal dendrites of BIN neurons were only sparsely covered by GAD+ nerve terminals. In this respect, BIN neurons were distinct from cerebellar nuclear neurons, whose cell bodies and proximal dendrites are densely innervated by GAD+ synaptic terminals from Purkinje cells axons (compare Fig. 2b and e). Analysis of GAD/ChAT double labelling in the floccular complex showed that ChAT+ axons in the granule cell layer were GAD+ (Fig. 2c), supporting the notion that ChAT+ fibers in these lobes are axons from BIN neurons. Moreover, these GAD+ChAT+ labeled axonal projections were morphologically distinct from ChAT+ mossy fibers in the nodulus that were GAD-negative (Fig. 2e). In contrast to previous monkey studies suggesting that ChAT+ fibers in the flocculus represent mossy fibers from the medial vestibular and the prepositus hypoglossal nuclei (Barmack et al., 1992a; Barmack et al., 1992b), we found virtually no ChAT+ fibers in the macaque flocculus that showed the typical mossy fiber morphology.

ChAT+ boutons in the flocculus/ventral paraflocculus did not stain positive for the mGluR2 metabotropic glutamate receptor (Fig. 2f), which is expressed by the majority of cerebellar Golgi cells, and is present on a large proportion of the GABAergic nerve terminals in the glomeruli (Neki et al., 1996; Watanabe et al., 1998; Simat et al., 2007). Notably, glomeruli with ChAT+ boutons always also contained mGluR2+ boutons (Fig. 2f), indicating that BIN axon terminals complement Golgi cell axonal terminals in the same glomeruli. Triple staining of ChAT and mGluR2 with antibodies against VIAAT (vesicular inhibitory amino acid transporter, also termed vesicular GABA transporter, VGAT) to outline GABAergic/glycinergic inhibitory nerve terminals, showed that ChAT+ boutons, like mGluR2+ boutons, were VIAAT+ (Fig. 2g), further indicating that ChAT+ fibers in the macaque flocculus are GABAergic. In addition to ChAT+mGluR2-VIAAT+ and ChAT-mGluR2+VIAAT+ boutons we also found ChAT-mGluR2-VIAAT+ boutons in the floccular glomeruli (Fig. 2g). Analysis of 50 floccular glomeruli in ChAT/VIAAT/mGluR2 triple-stained sections showed that about two-thirds (64 ± 2 %; mean ± SE) of the VIAAT+ boutons were ChAT-mGluR2+, while about one-third of the VIAAT+ boutons were mGluR2-, consisting of ChAT+mGluR2- (21 ± 1.4%) and ChAT-mGluR2- (15 ± 1.7%) boutons. We also performed triple staining of ChAT and VIAAT with VGluT1 to outline mossy fiber nerve endings (rosettes). This staining indicated that the distribution of ChAT+VIAAT+ boutons in floccular glomeruli resembles that of ChAT-VIAAT+ boutons (Fig. 2h). Together these

data indicate that a portion of inhibitory boutons in the macaque floccular glomeruli does not arise from mGluR2+ Golgi cells, and that about half of these mGluR2- boutons represent axon terminals from ChAT+ BIN neurons. For comparison, in the dorsal paraflocculus, which is not innervated by BIN afferents, we found more than 90% (94 ± 1%) of VIAAT+ boutons in the glomeruli to be mGluR2+.

In ChAT/VIAAT/mGluR2 stained sections we also noted ChAT+VIAAT+ boutons in glomeruli with a dendritic brush of unipolar brush cells (UBCs), which also may stain positive for mGluR2 (Jaarsma et al., 1998). Double labeling for ChAT and calretinin, which outlines a subset of UBCs (Sekerkova et al., 2014), showed the presence of ChAT+ boutons surrounding calretinin+ UBC brushes (Fig. 2i). However, we also found calretinin+ brushes that were not surrounded by ChAT+ boutons. This was particularly evident in a region of the ventral paraflocculus that shows a dramatic enrichment of UBCs and virtually no ChAT+ fibers (Fig. 2j). These data indicate that ChAT+ boutons do not have a simple all or none relationship with glomeruli containing UBC dendritic brushes.

3.3 ChAT-staining outlines the BIN in human cerebellum

To examine whether a BIN-like population of neurons also occurs in other species, we first examined human cerebellum. Using ChAT staining, we found a population of ChAT+ neurons in the basal white matter, reminiscent of BIN neurons in macaque (Fig. 3a,b). ChAT+ neurons were distributed in an area extending from the nodulus to the peduncles of the flocculus and the accessory paraflocculus (i.e. the human homologue of the macaque ventral paraflocculus; Voogd et al., 2012), ChAT+ neurons being most abundant near the base of the floccular peduncle (Fig. 3a,b). As in macaque, these ChAT+ neurons showed variable morphologies, had moderately large cell bodies (area = 533 ± 31 μm^2, 281-770; mean ± SE, range, n=20 cells), and stained positive for GAD (Fig. 3c,d). These data indicate that also in human cerebellum the BIN can be outlined using ChAT and GAD staining. Based on analysis of 1 out of 10 sections we estimate that about 5000 ($4.6 \pm 0.7*10^3$; Mean ± SE, n= 2) ChAT+ BIN neurons occur on each side of the cerebellum in human. The quality of the GAD staining did not allow counting of GAD+ BIN cells in human series.

As in macaque, ChAT+ fibers emanating from the human BIN were oriented towards the white matter of the flocculus and the accessory paraflocculus, and the flocculus/accessory paraflocculus showed a correspondingly high density of ChAT+ fibers in the white matter as well as a dense network of ChAT+ beaded fibers in the granule cell layer (Fig. 3e,f). However, in contrast to macaque, the human cerebellum also showed a subset of Golgi cells that were ChAT+ (Fig. 3f,g; see also de Lacalle et al., 1993), and, hence, ChAT+ innervation in the human flocculus/accessory paraflocculus may also derive from Golgi cells. The overall density of granular layer ChAT+ innervation in these lobules was higher than in other lobules. A particularly high density of ChAT+ fibers occurred in the areas of the floccular granule cell layer that contained ChAT+ Golgi cells (Fig.

3f), suggesting that in these areas ChAT+ axons are from both BIN neurons and Golgi cells. We were not able to further characterize the identities of ChAT+ boutons in the human floccular complex with reliable mGluR2 and VIAAT immuno-staining, probably due to limited possibilities of fixation and antigen epitope preservation of our human brain specimen.

3.4 Retrograde tracing and GAD-staining outlines the BIN in rat cerebellum

To further examine the occurrence of BIN neurons in other species we moved to rat. No ChAT+ neurons are present in the white matter of rat cerebellum (Jaarsma et al., 1996; Jaarsma et al., 1997). However, following floccular cortical injections with cholera toxin B subunit (CTB) (Ruigrok, 2003), we identified retrogradely labeled neurons in the hilus and the white matter of the ipsilateral flocculus (Fig. 4a-c). These retrogradely labeled neurons occurred throughout the rostro-caudal extent of the floccular white matter (Fig. 4a), were moderately large in size, and had multipolar and fusiform morphologies (Fig. 4b,c) reminiscent of macaque BIN neurons. Furthermore, these retrogradely labeled white matter neurons were all GAD+ (Fig. 4d). Based on their localization in the white matter and their similarities with macaque BIN neurons, we designate these neurons the rat homologues of macaque BIN neurons (Ruigrok, 2003). Notably, no retrogradely labeled BIN neurons occurred in an animal where the injection was centered in the ventral paraflocculus (e.g. case 902 in Ruigrok, 2003).

The rat BIN neurons could also be identified in thionin and NeuN stained sections, based on their size and localization in the white matter (Fig. 4c,e). Based on CTB tracing, GAD/NeuN staining and morphological criteria we propose that the BIN area in rat is rostro-medially delimited by the medial and inferior cerebellar peduncles, and more caudo-medially by the lateral cerebellar nuclei and group Y (Fig. 4a). Ventro-medially some BIN neurons may populate the cochlear nuclear superficial granule cell layer that borders the floccular white matter (Fig. 4a,b). Based on counting of GAD/NeuN and thionin stained serial sections, we estimate that in rat there are about 600-700 ($0.66 \pm 0.06*10^3$; Mean ± SE, n= 3) BIN neurons per side. We also estimated the number of retrogradely labeled BIN neurons in three animals following CTB injections in the floccular cortex (rat #798, rat #802 and rat #836; Ruigrok, 2003). Importantly, although injection areas covered less than 20% (15 ± 2%, mean ± SE) of the floccular granule cell layer, more than 70% (78 ± 5%) of BIN neurons were retrogradely labeled. These data suggest that projections from multiple BIN neurons converge on the same portion of the granule cell layer.

3.5 Electrophysiological characterization of rat BIN neurons in acute slices

To electrophysiologically characterize the BIN cells, we performed whole cell recording in acute transverse slices of rat cerebellar cortex. After recordings, cells were filled with neurobiotin for morphological analysis (Fig. 5a,b). Consistent with immunohistological data neurobiotin-filled BIN neurons showed fusiform or polygonal cell bodies with long dendrites that extend in the white matter

from opposite poles of the cell. In 3 of 7 cells dendritic branches also extended into the granule cell layer to reach the Purkinje cell layer (Fig. 5a,b). The axon extended from the cell body or a proximal dendrite and produced multiple branches, many of which left the slice. In 2 of 7 cells we could trace several axonal branches innervating a substantial portion of the granule cell layer within the slice (Fig. 5a,b). The axonal branches produced a network of fine beaded fibers with multiple ramifications (Fig. 5b-d). Co-staining for mGluR2 and VGluT1 confirmed that the neurobiotin-labeled axons do not stain for mGluR2, but co-distribute with mGluR2+ axonal profiles in glomeruli identified with VGluT1-staining of the mossy fiber rosettes (Fig. 5c,d). Typically, individual branchlets of the BIN-axon innervated 10-20 glomeruli with 2-5 boutons/per glomerulus (Fig. 5c,d). These data are consistent with the notion emerging from our tracing experiments that individual BIN neurons have diffuse widespread projections, innervating large proportions of the floccular granule cell layer.

Cell attached recordings from 7 morphologically validated BIN neurons indicated that they were silent (n=5) or fired at low frequency (8.4 and 5.6 Hz respectively). The capacitance of the cells was 48 ± 10 pF (15-88; Mean ± SE, ranges, n = 7). We next determined their excitability in current clamp mode. Increasing depolarizing current injections with 20 pA increment triggered increased firing rates (Fig. 5e,f) with a rheobase current of 50 ± 10 pA (Mean ± SE, n=7), action potential (AP) threshold of -43 ± 2 mV (Fig. 5g), peak AP amplitude of 93 ± 6 mV, AP rise and decay times of 0.55 ± 0.02 and 1.18 ± 0.05 ms, respectively, and afterhyperpolarization amplitude of 12 ± 1 mV. Whole-cell voltage-clamp recoding uncovered spontaneous EPSC (sEPSC) in BIN cells (Fig. 5h-j), with sEPSC amplitudes of 17.69 ± 3.13 pA and frequencies of 3.93 ± 1.14 Hz. Together the data indicate that BIN neurons are readily excitable, receive excitatory input (see below), but show a low level of intrinsic firing activity in acute slices.

3.6 Necab1outlines BIN neurons in mouse flocculus

To further characterize the BIN in rodents we performed retrograde CTB tracing in GlyT2GFP mice that express GFP under control of the GlyT2 gene promoter to label glycinergic neurons (Zeilhofer et al., 2005). We found that all retrogradely labeled BIN neurons were GFP+, indicating that BIN neurons are also glycinergic (Fig. 6a, b). Counting of serial GlyT2GFP sections indicated that mice have about 300 ($0.33 \pm 0.02*10^3$, mean ± SE, n = 6 flocculi from 3 animals) BIN neurons per side. Consistent with data from rat, CTB retrograde tracing in mouse showed that, while the injection areas covered less than 20%, (12 ± 3%, n = 3) of the floccular granule cell layer, more than 60% (63 ± 2%) of GFP+ BIN neurons were retrogradely labeled, indicative of widespread overlapping projection of BIN neurons. Together the data indicate that also in mice BIN neurons are distributed throughout the hilus and white matter of the flocculus.

As in macaque and rat, BIN neurons in the floccular white matter mice can be differentiated from Golgi cells in the floccular granule cell layer based on the absence of mGluR2 immunoreactivity

(Fig. 6c). BIN neurons stained positive for the cholinergic muscarinic M2 receptor (Fig. 6d), which is expressed in cerebellar Golgi cells in multiple mammalian species (Jaarsma et al., 1995; Jaarsma et al., 1997). To further identify genes that are expressed by BIN neurons, we used the AGEA (Anatomic Gene Expression Atlas) viewer modus of Allen Brain Atlas that examines gene expression in user defined neuroanatomical areas. We screened nearly 2000 genes for distinct signal in intermediate-large cells in the white matter of the anterior flocculus. In accord with our immunohistological data, no visible signal occurs in the floccular white matter of *mGluR2* mRNA labeled sections, whereas sections stained for *Gad1 (Gad67)*, *Gad2 (Gad65)*, *GlyT2 (Slc6A5)* and *ChRM2* mRNA show labelling of intermediate-sized cells in the floccular white matter, indicative of labelling of BIN neurons (Fig. 6e). Of 89 genes with distinct labelling of BIN neurons identified in our screen, the majority (85 of 89) showed similar expression in granule cell layer interneurons, while showing variable expression in other cerebello-cortical neuronal populations. Examples of genes that like *GlyT2* and *ChRM2* are expressed in both BIN neurons and granule cell layer interneurons, include acetylcholine esterase (*AChE*) and *Lgi2* (Fig. 6e). Out of the 2000 genes examined, we identified only four genes with distinct expression in BIN neurons and no apparent expression in granule cell layer interneurons in the flocculus. For one of these, *Necab1* (N-terminal EF-hand calcium Binding protein 1) expression in BIN neurons was confirmed by immunohistology (Fig. 6f,g): Analysis of Necab1 immunostaining in GlyT2GFP mice shows that all GFP+ neurons in the floccular hilus and white matter, stain positive for Necab1, while other floccular cells, including GlyT2+ Golgi and Lugaro cells show no or very weak staining for Necab1 (Fig. 6f). Accordingly, BIN neurons identified by retrograde CTB-tracing were always strongly Necab1+ (Fig. 6g). Necab1 immunohistology also showed that BIN neurons may have one or more dendritic branches extending into the granule cell layer (Fig. 6f), consistent with data from rat neurobiotin-filled BIN neurons. Together, the data indicate that Necab1 selectively outlines BIN neurons in the mouse flocculus, consistent with the idea that they represent a specific class of floccular neurons.

3.7 Absence of Necab1+ and Neurogranin+ Golgi cells in mouse flocculus

While granule cell layer interneurons in the flocculus show no or very weak Necab1 expression, a substantial subset of granule cell layer interneurons in other cerebellar lobules stained positive for Necab1 (Fig. 6f). The Necab1+ granule cell layer interneurons included both GlyT2GFP+ and GlyT2GFP- neurons (Fig. 6f). These data indicate that Necab1 outlines one or more subclasses of granule cell layer interneurons that are absent in the flocculus. To further characterize Necab1+ granule cell layer interneurons, and differences between the flocculus and other cerebellar lobules we compared the distribution of Necab1 with that of mGluR2 and neurogranin in sections from GlyT2GFP mice. A previous study focusing on lobules 4-6 of the vermis (Simat et al., 2007) showed that several subclasses of granule cell layer interneurons can be differentiated on the basis of

differential expression of these markers, including a population of GlyT2GFP+mGluR2+neurogranin+ cells (designated type 1 Golgi cells), two populations that are GlyT2GFP+mGluR2+, but neurogranin- (type 2 and 3 Golgi cells), GlyT2GFP-GluR2-neurogranin+ cells (type 4 Golgi cells), and GlyT2GFP+ cells that are neurogranin-mGluR2- (representing Lugaro and globular cells). Consistent with this classification we found that in lobule 4-5 of the vermis (verm4/5) neurogranin occurred in GlyT2GFP+ as well as GlyT2GFP- Golgi cells (Fig. 7a), and that GlyT2GFP-/neurogranin+ cells were negative for mGluR2 (type 4 Golgi cells), while GlyT2GFP+/neurogranin+ Golgi cells were mGluR2+ (type 1 Golgi cells). However, no neurogranin+ Golgi cells occurred in the flocculus, and furthermore also BIN neurons stained negative for neurogranin (Fig. 7b). Like neurogranin, Necab1 in verm4/5 occurred in either GlyT2GFP-/mGluR2- (potentially type 4 Golgi cells) or GlyT2GFP+/mGluR2+ (potentially type 1 Golgi cells), but not in GlyT2GFP+/mGluR2- cells (Lugaro/globular cells) (data not shown). Double labeling for Necab1 and neurogranin showed consistent codistribution of neurogranin and Necab1 in GlyT2GFP- (type 4) Golgi cells, but incomplete colocalization in GlyT2GFP+ Golgi cells (Fig. 7c). These data indicate that Necab1 is expressed in type 4 Golgi cells, to variable extent is expressed by other Golgi cell subtypes, but is not expressed in Lugaro/globular cells.

We further characterized differences in Golgi cells between the flocculus and verm4/5 using an antibody against Lgi2. Lgi2-immunostaining occurred in granule cell layer interneurons as well as BIN neurons, in accord with mRNA expression data from Allan brain atlas (Fig. 6e). Lgi2/mGluR2 and Lgi2/neurogranin double labeling in GlyT2GFP mice indicated that in verm4/5 Lgi2 is expressed in all Golgi cells, but not in Lugaro/globular cells: thus, in Lgi2/mGluR2 labeled sections, Lgi2-immunostaining outlines GlyT2GFP+mGluR2+ cells (type 1-3 Golgi cells) and GlyT2GFP-mGluR2- cells (potentially type 4 Golgi cells), but is not present in GlyT2GFP+mGluR2- cells (Lugaro/globular cells) (data not shown). Lgi2/neurogranin staining showed that GlyT2GFP-Lgi2+ cells all stain positive for neurogranin (Fig. 7d,e) and indeed represent type 4 Golgi cells. Consistent with the notion that type 4 Golgi cells do not occur in the flocculus we found that all Lgi2+ cells in the floccular granule cell layer were GlyT2+mGluR2+, with the exception of sporadic GlyT2GFP+ cells that like BIN neurons are Necab1+ (Fig. 7f,g). Cell counts in Lgi2/Necab1/GlyT2GFP and Lgi2/neurogranin/GlyT2GFP labeled sections indicated that the density of Lgi2+ Golgi cells is slightly, but non-significantly ($p = 0.09$; unpaired 2-tailed *t*-test) higher in verm4/5 compared to the flocculus, with 227 ± 17 (Mean ± SE, n=3 animals) Lgi2+ cells/mm^2 in verm4/5 and 187 ± 11 (n=4) Lgi2+ cells/mm^2 in the floccular granule cell layer, respectively. In verm4/5 87% (197 ± 15) of the Lgi2+ Golgi cells were GlyT2GFP+ representing type 1-3 Golgi cells, whereas in the flocculus all Lgi2+ cells were GlyT2+. In sum, our comparison of Golgi cells between verm4-5 and flocculus using established (mGluR2, neurogranin, GlyT2) and novel markers (Lgi2, Necab1) of (subsets of) Golgi cells, uncovered differences in the neurochemical identities of Golgi cells in the flocculus versus the

anterior vermis (Simat et al., 2007). In particular, the absence of neurogranin+, Necab1+, and Lgi2+GlyT2GFP- Golgi cells in the flocculus indicates that type 4 Golgi cells are not present in the flocculus, all Golgi cells being mGluR2+GlyT2+.

3.8 BIN neurons innervate granule cells dendrites in floccular glomeruli

Based on analysis of BIN nerve terminals in macaque and rat, we anticipate that BIN axons provide inhibitory input to granule cell dendrites, and complement inhibitory input from Golgi cells in floccular glomeruli. To further examine the axonal projections of BIN neurons we injected AAV-GFP viral particles into the white matter and hilus of the flocculus of mice (Fig. 8a). We obtained 7 injections centered in the hilus of the flocculus infecting BIN neurons and resulting in a variable degree of axonal labelling in the ipsilateral flocculus (Fig. 8b,c). Labeled axons were morphologically distinct from mossy fibers, and form a plexus of thin fibers with multiple VIAAT-positive nerve terminals (Fig. 8c) resembling BIN fibers in macaque (Fig. 2) and rat (Fig. 5a-c). No GFP+VIAAT+ labeled axons occurred in the flocculus in case of more dorsal and medial injections that targeted the cerebellar nuclei, but did not target BIN neurons. The highest densities of labeled fibers occurred in experiments, where also BIN neurons in the floccular white matter were infected (Fig. 8b).

To characterize the post-synaptic target of AAV-GFP labeled BIN axons, we performed transmission electron microscopy of anti-GFP immunoperoxidase histochemistry with diaminobenzidine (DAB) as a substrate. Consistent with GFP fluorescence, DAB precipitate was associated with thin axonal profiles and presynaptic boutons with diameters ranging from 1 to 2 µm. Labeled axon terminals were localized in glomeruli (Fig. 8d). Analysis of 40 labeled axon terminals, revealed multiple synaptic contacts with granule cell dendrites (Fig. 8d). Post-embedding immunogold labelling for GABA showed that DAB-labeled profiles in all occasions (n=30) are enriched in GABA-immunoreactivity (Fig. 8e,f) Together the data indicate that BIN axons like Golgi cell axon terminals (Palay and Chan-Palay, 1974; Dugue et al., 2005; Pietrajtis and Dieudonné, 2013; Mapelli et al., 2014) primarily innervate granule cell dendrites.

3.9 BIN inhibitory input complements mGluR2+ Golgi axon terminals in glomeruli in the mouse flocculus

Immunostaining of AAV-GFP labeled sections for VIAAT, mGluR2 and VGluT1 showed that GFP+ BIN axon terminals always are mGluR2-negative, but co-distribute with VIAAT+mGluR2+ boutons in the same glomeruli (Fig. 8g,h). In addition, the same glomeruli also contained VIAAT+ terminals that are both mGluR2- and GFP-negative (Fig. 8g). To obtain an estimate of the proportion of mGluR2+ Golgi versus BIN axon terminals in the floccular granule cell layer we determined the proportion of VIAAT+ boutons labeled by either GFP or mGluR2 in confocal stacks from the three AAV-GFP injections that yielded the highest level of BIN axonal labelling (i.e. VBIN2, VBIN3,

VBIN5). This analysis showed that 10-20% of the area labeled by VIAAT was GFP+ whereas 50-60% of the VIAAT+ area was mGluR2+ (Fig. 8i). For comparison, we analyzed the proportion of mGluR2+ VIAAT+ boutons in the nodulus and lobules 3 and 4/5 of the anterior vermis (Fig. 8j,k). In the anterior vermis, more than 90-95% of VIAAT+ area was mGluR2+ (Fig. 8j,k), consistent with the notion that inhibitory axons in the glomeruli primarily derive from mGluR2+ Golgi cells (Ohishi et al., 1994; Watanabe et al., 1998; Simat et al., 2007), while in the nodulus about 70% of the VIAAT+ area van mGluR2+ (Fig. 8k). The large proportion (40-50%) of VIAAT+mGluR2- boutons in the floccular granule cell layer as compared to the anterior vermis and the nodulus, can at least in part be explained by the presence of innervation from BIN neurons. In accord with data from macaque flocculus, these data indicate that BIN inhibitory input represents a significant complement of inhibitory input from Golgi cells in the floccular granule cell layer (Fig. 8l).

3.10 Rodent BIN neurons receive excitatory input from the rostro-medial medullary reticular formation

Staining for markers of inhibitory (VIAAT, GAD) and excitatory (VGluT1, VGluT2) nerve terminals, revealed that BIN neurons have a large number of VGluT2-positive boutons contacting their cell body and proximal dendrites (Fig. 9a) consistent with our electrophysiological analysis showing sEPSC in BIN neurons (Fig. 5h-j). To learn about the origin of this excitatory input, we set out tracing experiments in mouse. VGluT2 is present in climbing fibers and multiple populations of mossy fibers (Hioki et al., 2003) raising the possibility that BIN neurons are innervated by collaterals of climbing or mossy fibers. To test this possibility, we injected anterograde tracer (biotin dextran amine 10 kDa, BDA) in the inferior olive, i.e. the source of climbing fibers, and in brainstem nuclei known to provide mossy fiber input to the flocculus, including the vestibular nuclei and the prepositus hypoglossal nucleus (Ruigrok, 2003). However, none of these injections resulted in labelling of fibers contacting BIN neurons, despite abundant climbing fiber and mossy fiber labelling, respectively (data not shown). Instead a systematic anterograde tracing approach with injections throughout the medulla oblongata and the pontine reticular formation, revealed that BDA injection in the rostro-medial medullary reticular formation resulted in labeling of fibers innervating BIN neurons (Fig. 9b-e). We obtained 7 BDA injections that resulted in labeling of beaded fibers contacting the cell bodies and proximal dendrites of a substantial portion (>30%) of BIN neurons. These injections all targeted the medio-dorsal aspect of the medullary gigantocellular reticular nucleus (Gi). In 4 of 7 cases injections also included the dorsal paragigantocellular reticular nucleus (DPGi) dorsal of the Gi. However, 2 injection that targeted the DPGi, but not the Gi, resulted in labeled fibers on less than 4% of BIN neurons, indicating that afferents predominantly arise in the Gi. Similarly, BDA injections in the ventral aspect of the Gi, the pontine reticular formation rostral of the Gi, or the caudal aspect of the Gi resulted in no or minimal labeling of BIN afferents, substantiating the medio-dorsal Gi as the main

source of BIN afferents. Importantly, the injections restricted to the medio-dorsal Gi that resulted in substantial labelling of BIN afferents (e.g. experiments #1541, #1606 and #1536) all produced negligible mossy fiber staining, supporting the notion that fibers innervating the cell bodies of BIN neurons do not represent mossy fiber collaterals. In all experiments labeled BIN afferent fibers were observed bilaterally, even when the injection was clearly unilateral. In addition, we observed that individual afferents may innervate several BIN neurons, and typically produce multiple (5-32) consecutive swellings on the cell body and proximal dendrites of individual BIN neurons (Fig. 9c,e). Double labelling for VGluT2 indicated that these axonal swellings in all occasions were VGluT2+ (Fig. 9e). In all neurons systematically examined for codistribution of BDA and VGluT2 (30 of 30 cells) we found that BDA+VGluT2+ boutons on BIN neurons were complemented by BDA-VGluT2+ boutons (Fig. 9e). This observation indicates that individual BIN neurons are innervated by multiple excitatory axons. To further demonstrate that VGluT2+ axon terminals innervating BIN neurons arise from neurons in the medio-dorsal Gi, we injected AAV-flex-GFP viral particles in the Gi of VGluT2-Cre mice in order to express GFP selectively in VGluT2 expressing neurons. Consistent with BDA tracing these injections resulted in bilateral GFP+ beaded fibers that made multiple synaptic connections with BIN neurons (Fig. 9f).

Next, to visualize the cells of origin of the BIN afferents in the Gi, we performed retrograde tracing with cholera toxin ß subunit (CTB). Comparison of CTB injections centered in the hilus of the flocculus (n=2) with injections in the floccular cortex (n=4), uncovered a population of intermediate-size (length =14 to 22 μm) polygonal CTB-labeled neurons in the dorsal Gi following hilar, but not cortical CTB injections (Fig. 9g). Consistent with anterograde tracing experiments, retrogradely-labeled neurons occurred both ipsi- and contralateral. Large neurons, characteristic for the Gi were not retrogradely labeled. The presence of intermediately sized VGluT2+ neurons in the Gi is consistent with *VGluT2* mRNA expression data documented in Allen brain atlas (Lein et al., 2007) showing high levels of *VGluT2* mRNA staining in both very large and small-to-intermediate size neurons in the Gi. We therefore propose that BIN neurons receive bilateral excitatory input from intermediately sized neurons in the dorsal Gi. Together the data indicate that the BIN is part of a disynaptic afferent pathway to the floccular granule cell layer, consisting of glutamatergic fibers from the medullary reticular formation innervating BIN neurons that in turn provide inhibitory input to granule cells (Fig. 9h).

3.11 Variability in the distribution of BIN neurons across mammalian species.

On the basis of data from primates and rodent, the BIN can be defined as a population of GABA/glycinergic neurons in the white matter, that innervate the floccular granule cell layer. However, BIN neurons show a differential distribution in rodents and primates, i.e. a preferential localization in the floccular white matter in rodents, versus a more widespread and distant distribution

in the white matter between the floccular peduncle and the cerebellar nuclei in macaque and human. This raises questions about the presence and distribution of BIN neurons in other mammalian species. Our search for BIN neurons in rabbit cerebellum indicates that their identification in other species is not always straightforward. Thionin and GAD staining shows that in rabbit a low number of neurons is present in the white matter within and dorso-medial of the flocculus. Accordingly, analysis of sections from previous tracer experiments with small injections of the anterograde/retrograde tracer WGA-HRP in the floccular cortex (rabbits K227, K244, K358, K360; Tan et al., 1995) revealed no or sporadic retrogradely labeled cells in this area. However, further analysis of these experiments revealed retrogradely labeled cells in the white matter medial of the medial cerebellar peduncle (mcp), rostral of the cerebellar nuclei (Fig. 10a,b). Retrogradely labeled cells only occurred ipsilateral. Notably, in several occasions labeled cells occurred close to the granule cell layer of the anterior vermis (Fig. 10b). Importantly, GAD staining revealed GAD+ neurons with similar size and distribution in this region of the white matter (Fig. 10c,d). The GAD+ neurons showed morphologies reminiscent of BIN neurons in primates and rodent. Based on counting of serial sections, we estimate that on each side there are about 800 ($0.8 \pm 0.2 * 10^3$, mean ± SE, n=2) of these GAD+ neurons populating either the floccular or the anterior vermis white matter (Fig. 10c,d).

To further explore the variability in distribution of BIN neurons across mammalian species we searched for potential BIN neurons in ferret cerebellum. Analysis of thionin and GAD stained section showed that as in primates and rabbit there are only a few GAD+ neurons in the white matter of the ferret flocculus. However, a cluster of GAD+ neurons, reminiscent of BIN neurons, was present in the white matter of the transition zone between the flocculus and the ventral paraflocculus (Fig. 11). Caudo-dorsally this cluster is bordered by the lateral cerebellar nuclei. Like BIN neurons the neurons are moderately-large in size and show elongated fusiform or polygonal morphologies with dendrites emanating from two sides. With about 1000 ($1.1 \pm 0.1 * 10^3$, mean ± SE, n=2) neurons per side, their number is compatible with BIN neurons in other species. Together the data indicate that BIN neurons also occur in rabbit and ferret cerebellum, but show different distributions than in rodent and primates.

4. DISCUSSION

The BIN has been originally identified by Langer in macaque as a population of neurons that innervate the flocculus and the ventral paraflocculus (also designated floccular complex; Voogd et al., 2012), and is located in the basal white matter between the flocculus and the cerebellar nuclei (Langer et al., 1985; Langer, 1985). Although this finding was confirmed by others (Nagao et al., 1997a), the BIN has been largely neglected in the literature. In addition, in some studies (Gonzalo-Ruiz et al., 1988; Takikawa et al., 1998) the term BIN has been used for a group of neurons that does not overlap with the BIN originally defined by Langer (Langer, 1985). In these studies, 'BIN' neurons were found to project to pontine nuclei (Gonzalo-Ruiz et al., 1988) and to display saccade-related firing activity (Takikawa et al., 1998). However, the cells explored in these studies were localized medial of group Y, whereas BIN neurons identified by retrograde tracing localize lateral of group Y (see Fig 1 of this study, and Fig. 3 in Langer, 1985). In a recent human brain Atlas (Ding et al., 2016), the term BIcb (basal interstitial nucleus of the cerebellum) has been assigned to a population of large neurons in the roof of the 4th ventricle neurons (see Fig. 13 in Ding et al., 2016). In this study, there is no reference to the study of Langer (Langer, 1985), and it is not clear whether the BIcb was intended to represent the human homologue of the macaque BIN (Ding et al., 2016). On the basis of our data, we propose to reserve the term BIN (or BICb) for the population of neurons originally defined by Langer on the basis of retrograde tracing from the flocculus (Langer et al., 1985; Langer, 1985). Our data indicate that these neurons represent a novel GABAergic cerebellar neuron that can be found in multiple mammalian species beyond macaque, including human, rat, mouse, rabbit and ferret (Table 2). Distinctive properties of BIN neurons are the following: they are moderately-sized GABAergic neurons localized in the white matter; they innervate floccular granule cells; and they receive excitatory input from the medullary reticular formation. BIN neurons represent a second source of inhibition of floccular granule cells, complementing inhibitory input from Golgi cells (Fig. 9h).

We found that BIN neurons in macaque stain positive for GAD and ChAT (Figs 1 and 2) and that ChAT staining can also be used to outline the BIN in human cerebellum (Fig. 3). ChAT staining did not label BIN neurons in the other species investigated, i.e. rat, mouse, rabbit and ferret, but in these species, we identified homologous populations of neurons based on the following criteria: their localization in the white matter, their size and elongated morphologies with dendrites emanating from the two ends, their retrograde labeling after tracer injection in the flocculus, and their immunoreactivity for GAD (Figs 4, 6, 10, 11). Our data indicate that the distribution of BIN neurons shows variability across species, varying from the floccular white matter in rat and mouse, to a relatively condensed distribution in the white matter dorso-medial of the flocculus in ferret, and more widespread distributions in rabbit and primates.

A search in Allen Brain Atlas to identify molecular markers that could further aid in the identification of BIN neurons uncovered the calcium binding protein Necab1 as a marker for BIN neurons in mouse cerebellum (Fig. 6). However, Necab1 is not expressed by BIN neurons in other species. The interspecies heterogeneity of ChAT and Necab1 expression is not against our tenet that BIN neurons represent a single class of neurons across species for two reasons: First, Necab1 is also absent in rat BIN neurons, which are highly similar to mouse BIN neurons in distribution and morphology. Second, interspecies heterogeneity in the expression of neurochemical markers also occurs in other populations of cerebellar neurons, in particular Golgi cells that differentially express ChAT, neurogranin and calretinin in closely related species (Jaarsma et al., 1997; Geurts et al., 2001; Bastianelli, 2003; Singec et al., 2003; Eyre and Nusser, 2016). In addition to Necab1, we found other proteins that might serve as neurochemical markers for BIN neurons, although the majority of these, like GlyT2, muscarinic M2 receptor, Lgi2, and acetylcholine esterase (AChE) are also expressed by Golgi cells (Figs 6, 7). In fact, our data show that also Necab1, while not being expressed by Golgi cells in the flocculus, is expressed in a subset of Golgi cells in most other lobules (Figs 6, 7). Instead mGluR2 is a marker that differentiates BIN neurons from Golgi cells, as it is not expressed in BIN neurons (Figs 2, 5, 6, 8) while being expressed by the majority of cerebellar Golgi cells and their nerve terminals (Neki et al., 1996; Watanabe et al., 1998; Geurts et al., 2001; Simat et al., 2007). Furthermore, in mouse, we found that BIN neurons do not express neurogranin (Fig. 7), another Golgi cell marker that is expressed in at least 2 subpopulations of Golgi cells in mouse cerebellum, including a subpopulation of Golgi cells (type 4 Golgi cells) that does not express mGluR2 and GlyT2 (Singec et al., 2003; Simat et al., 2007). Importantly, by comparing the expression of a panel of Golgi cell markers between anterior vermis and the flocculus, we found that neurogranin+GlyT2-mGluR2- Golgi cells, while constituting 10-15% of the Golgi cells in the anterior vermis (Simat et al., 2007), are not present in the flocculus, (Fig. 7). These findings on the one hand point to differences in neurochemical identities between Golgi cells in the flocculus compared to the anterior vermis (Simat et al., 2007); and on the other hand, support our notion that mGluR2 may represent a useful marker to differentiate BIN neurons from Golgi cells in the flocculus .

Recently, an ascending GABAergic/glycinergic inhibitory projection from the cerebellar nuclei to the cerebellar cortex has been reported (Ankri et al., 2015). These nucleo-cortical inhibitory neurons differ from BIN neurons in at least two aspects: They do not express Necab1 and they innervate Golgi cells rather granule cells (Ankri et al., 2015). It has been suggested that these inhibitory nucleo-cortical neurons also innervate the floccular granule cell layer (see Fig. 2A of Ankri et al., 2015). However, we did not identify retrogradely labeled neurons in the cerebellar nuclei following CTB tracer injection in the flocculus. We, therefore, speculate that the floccular projections in the study of Ankri et al. (2015) derive from BIN neurons. The absence of inhibitory nucleo-cortical projections to the flocculus also is consistent with the absence of neurogranin+GlyT2-mGluR2- Golgi

cells in the flocculus (Fig. 7), representing a major target of this projection (Ankri et al., 2015). Taken together, although BIN neurons show resemblance with either Golgi cells or inhibitory nucleo-cortical neurons and probably derive from the same lineage, they are sufficiently distinct to consider them as a novel population of cerebellar neurons.

To characterize BIN axon terminals, we took advantage of their immunoreactivity for ChAT in macaque flocculus (Fig. 2) and we used AAV-GFP anterograde tracing in mice (Fig. 8). We found that BIN axon terminals to various degrees populate glomeruli in the floccular granule cell layer and complement mGluR2+ inhibitory input from Golgi cells. Electron microscopy of anterogradely labeled BIN axons in mouse provided direct demonstration that BIN axons innervate granule cell dendrites (Fig. 8d,e). Using confocal microscopy, we found examples of ChAT+ BIN axons innervating glomeruli with UBC brushes in macaque (Fig. 2i). So far, we did not obtain ultrastructural evidence of BIN axons making synaptic contacts with UBCs. We also used confocal microscopy to examine whether AAV-GFP traced BIN axons contact Golgi cells stained with antibodies against mGluR2 or muscarinic M2 receptor, but so far, we did not find conclusive examples of BIN axons contacting the cell body or dendrites of Golgi cells. Thus, granule cell dendrites represent a major target of BIN axons, while further work is needed to establish to what extent other granule cell layer neurons receive direct BIN input.

To obtain an idea about the relative contribution of inhibition by BIN axons in the floccular granule cell layer, we determined the proportion of ChAT+ inhibitory boutons in macaque flocculus, and the proportion of GFP+ inhibitory boutons in AAV- GFP anterograde tracing experiments in mice. These analyses indicated that at least 20% of inhibitory boutons in the floccular granule cell layer represent BIN axon terminals. Thus, in macaque flocculus about 20% of VIAAT+ boutons stain positive for ChAT, while in mice AAV-GFP injections resulted in GFP labelling of up to 20% of VIAAT+ boutons. However, the proportion of BIN axon terminals is likely to be higher in both macaque and mouse, in view of the presence of a population of ChAT- BIN neurons in macaque (Fig. 2a,b), and unlabeled BIN neurons in the AAV- GFP tracing experiments in mice. Analysis of the proportion of Golgi axon terminals on the basis of double labelling for VIAAT and mGluR2 metabotropic glutamate receptor, indicated that about 60% of VIAAT+ axon terminals in the floccular granule cell layer is from mGluR2+ Golgi cells. Instead the proportion of mGluR2+ boutons is higher in other lobules (up to 95% in the anterior vermis; Fig. 8j,k), consistent with previous data indicating that 85-90% of Golgi cells are mGluR2+ (Neki et al., 1996; Simat et al., 2007) and that toxin-mediated selective ablation of mGluR2+ Golgi cells results in almost complete loss of GABAergic boutons in the granule cell layer (Watanabe et al., 1998). The large proportion of mGluR2-VIAAT+ boutons in the floccular granule cell layer (about 40%) as compared to other lobules, at least in part can be explained by the presence BIN axons. mGluR2-VIAAT+ boutons also may derive from mGluR2- Golgi cells, but our data indicate that this type of Golgi cell does not occur in the flocculus (see

above). Purkinje cells may represent an additional source of inhibitory boutons in the granule cell layer (Guo et al., 2016) predominantly innervating Lugaro and globular cells (Simat et al., 2007), but double labelling for VIAAT and the Purkinje cell marker calbindin indicated that inhibitory boutons from Purkinje cells are rare in the floccular granule cell layer (<1% of VIAAT boutons). Taken together, our data indicate that about 60% of the VIAAT+ axon terminals in the floccular granule cell layer derive from mGluR2+ Golgi cells, while at least 20% and potentially up to 40% of the residual VIAAT+ axon terminals are from BIN neurons.

What could be the function of BIN neurons in the floccular circuitry? BIN axon terminals co-distribute with mGluR2+ Golgi cell axon terminals in the same glomeruli, and likely have complementary roles in controlling mossy fiber to granule cell signaling. Golgi cells receive excitatory granule cell and mossy fiber input and implement a local inhibitory feedback circuit that may control the precise timing and gain of granule cell firing (Cesana et al., 2013; Pietrajtis and Dieudonné, 2013; Valera et al., 2016). The distinctive feature of Golgi cells is their local dense axonal plexus that provides inhibitory input primarily to nearby granule cells, although some Golgi cells may have more distant projections (Pietrajtis and Dieudonné, 2013). BIN neurons instead project to large portions of the flocculus, and only produce a few axon terminals per glomerulus. This wiring pattern indicates that BIN neurons have a more global inhibitory role over widely distributed granule cells (Fig. 9h). We also show that BIN neurons receive bilateral glutamatergic input from a population of neurons in the medullary gigantocellular reticular formation. These fibers innervate the cell body and proximal dendrites of BIN neurons, and likely play an important role in controlling the activity of BIN neurons. Importantly, our data also indicate that BIN neurons are not innervated by collaterals from climbing and mossy fiber collaterals that innervate the floccular cortex, although at this point we can not exclude collateral projections on distal dendrites of BIN neurons. It had been anticipated by Langer that BIN neurons receive inhibitory input from floccular Purkinje cells (Langer, 1985). However, anterograde tracing experiments in macaque have shown that BIN neurons to not receive input from the flocculus (Nagao et al., 1997b). In accord with the idea that BIN neurons do not receive Purkinje cell input, our data indicate that BIN neurons are only innervated by calbindin-negative inhibitory boutons.

Together the data indicate that BIN neurons represent a diffuse inhibitory system of floccular granule cells that is controlled by a group of neurons in the medullary formation (Fig. 9h). Understanding the information conveyed by the medullary BIN afferents, will be critical for clarifying the role of the BIN neurons in the well-established role of the flocculus in eye movement control (Ito, 1982; De Zeeuw et al., 1995; Schonewille et al., 2006; Voogd et al., 2012; Voges et al., 2017). Importantly, future studies on the function of BIN neurons would benefit from experiments in multiple mammalian species to validate whether BIN neurons indeed represent a single class of prefloccular neurons with evolutionary conserved function.

References

Ankri L, Husson Z, Pietrajtis K, Proville R, Lena C, Yarom Y, Dieudonne S, Uusisaari MY. 2015. A novel inhibitory nucleo-cortical circuit controls cerebellar Golgi cell activity. Elife 4.

Arenz A, Bracey EF, Margrie TW. 2009. Sensory representations in cerebellar granule cells. Curr Opin Neurobiol 19(4):445-451.

Barmack NH, Baughman RW, Eckenstein FP. 1992a. Cholinergic innervation of the cerebellum of rat, rabbit, cat, and monkey as revealed by choline acetyltransferase activity and immunohistochemistry. J Comp Neurol 317(3):233-249.

Barmack NH, Baughman RW, Eckenstein FP, Shojaku H. 1992b. Secondary vestibular cholinergic projection to the cerebellum of rabbit and rat as revealed by choline acetyltransferase immunohistochemistry, retrograde and orthograde tracers. J Comp Neurol 317(3):250-270.

Bastianelli E. 2003. Distribution of calcium-binding proteins in the cerebellum. Cerebellum (London, England) 2(4):242-262.

Boele HJ, Koekkoek SK, De Zeeuw CI, Ruigrok TJ. 2013. Axonal sprouting and formation of terminals in the adult cerebellum during associative motor learning. J Neurosci 33(45):17897-17907.

Cerminara NL, Lang EJ, Sillitoe RV, Apps R. 2015. Redefining the cerebellar cortex as an assembly of non-uniform Purkinje cell microcircuits. Nat Rev Neurosci 16(2):79-93.

Cesana E, Pietrajtis K, Bidoret C, Isope P, D'Angelo E, Dieudonne S, Forti L. 2013. Granule cell ascending axon excitatory synapses onto Golgi cells implement a potent feedback circuit in the cerebellar granular layer. J Neurosci 33(30):12430-12446.

Chabrol FP, Arenz A, Wiechert MT, Margrie TW, DiGregorio DA. 2015. Synaptic diversity enables temporal coding of coincident multisensory inputs in single neurons. Nature neuroscience 18(5):718-727.

Davie JT, Clark BA, Hausser M. 2008. The origin of the complex spike in cerebellar Purkinje cells. J Neurosci 28(30):7599-7609.

de Lacalle S, Hersh LB, Saper CB. 1993. Cholinergic innervation of the human cerebellum. J Comp Neurol 328(3):364-376.

De Zeeuw CI, Hoebeek FE, Bosman LW, Schonewille M, Witter L, Koekkoek SK. 2011. Spatiotemporal firing patterns in the cerebellum. Nat Rev Neurosci 12(6):327-344.

De Zeeuw CI, Ten Brinke MM. 2015. Motor Learning and the Cerebellum. Cold Spring Harb Perspect Biol 7(9):a021683.

De Zeeuw CI, Wylie DR, Stahl JS, Simpson JI. 1995. Phase relations of Purkinje cells in the rabbit flocculus during compensatory eye movements. J Neurophysiol 74(5):2051-2064.

Dean P, Porrill J, Ekerot CF, Jorntell H. 2010. The cerebellar microcircuit as an adaptive filter: experimental and computational evidence. Nat Rev Neurosci 11(1):30-43.

Ding SL, Royall JJ, Sunkin SM, Ng L, Facer BA, Lesnar P, Guillozet-Bongaarts A, McMurray B, Szafer A, Dolbeare TA, Stevens A, Tirrell L, Benner T, Caldejon S, Dalley RA, Dee N, Lau C, Nyhus J, Reding M, Riley ZL, Sandman D, Shen E, van der Kouwe A, Varjabedian A, Write M, Zollei L, Dang C, Knowles JA, Koch C, Phillips JW, Sestan N, Wohnoutka P, Zielke HR, Hohmann JG, Jones AR, Bernard A, Hawrylycz MJ, Hof PR, Fischl B, Lein ES. 2016. Comprehensive cellular-resolution atlas of the adult human brain. J Comp Neurol 524(16):3127-3481.

Dugue GP, Dumoulin A, Triller A, Dieudonne S. 2005. Target-dependent use of co-released inhibitory transmitters at central synapses. J Neurosci 25(28):6490-6498.

Eyre MD, Nusser Z. 2016. Only a Minority of the Inhibitory Inputs to Cerebellar Golgi Cells Originates from Local GABAergic Cells. eNeuro 3(2).

Gao Z, Proietti-Onori M, Lin Z, Ten Brinke MM, Boele HJ, Potters JW, Ruigrok TJ, Hoebeek FE, De Zeeuw CI. 2016. Excitatory Cerebellar Nucleocortical Circuit Provides Internal Amplification during Associative Conditioning. Neuron 89(3):645-657.

Gao Z, van Beugen BJ, De Zeeuw CI. 2012. Distributed synergistic plasticity and cerebellar learning. Nat Rev Neurosci 13(9):619-635.

Geurts FJ, Timmermans J, Shigemoto R, De Schutter E. 2001. Morphological and neurochemical differentiation of large granular layer interneurons in the adult rat cerebellum. Neuroscience 104(2):499-512.

Gonzalo-Ruiz A, Leichnetz GR, Smith DJ. 1988. Origin of cerebellar projections to the region of the oculomotor complex, medial pontine reticular formation, and superior colliculus in New World monkeys: a retrograde horseradish peroxidase study. J Comp Neurol 268(4):508-526.

Guo C, Witter L, Rudolph S, Elliott HL, Ennis KA, Regehr WG. 2016. Purkinje Cells Directly Inhibit Granule Cells in Specialized Regions of the Cerebellar Cortex. Neuron 91(6):1330-1341.

Harris JA, Oh SW, Zeng H. 2012. Adeno-associated viral vectors for anterograde axonal tracing with fluorescent proteins in nontransgenic and cre driver mice. Curr Protoc Neurosci Chapter 1:Unit 1 20 21-18.

Harvey RJ, Napper RM. 1988. Quantitative study of granule and Purkinje cells in the cerebellar cortex of the rat. J Comp Neurol 274(2):151-157.

Hioki H, Fujiyama F, Taki K, Tomioka R, Furuta T, Tamamaki N, Kaneko T. 2003. Differential distribution of vesicular glutamate transporters in the rat cerebellar cortex. Neuroscience 117(1):1-6.

Huang CC, Sugino K, Shima Y, Guo C, Bai S, Mensh BD, Nelson SB, Hantman AW. 2013. Convergence of pontine and proprioceptive streams onto multimodal cerebellar granule cells. Elife 2:e00400.

Ito M. 1982. Cerebellar control of the vestibulo-ocular reflex--around the flocculus hypothesis. Annu Rev Neurosci 5:275-296.

Jaarsma D, Dino MR, Cozzari C, Mugnaini E. 1996. Cerebellar choline acetyltransferase positive mossy fibres and their granule and unipolar brush cell targets: a model for central cholinergic nicotinic neurotransmission. J Neurocytol 25(12):829-842.

Jaarsma D, Dino MR, Ohishi H, Shigemoto R, Mugnaini E. 1998. Metabotropic glutamate receptors are associated with non-synaptic appendages of unipolar brush cells in rat cerebellar cortex and cochlear nuclear complex. J Neurocytol 27(5):303-327.

Jaarsma D, Levey AI, Frostholm A, Rotter A, Voogd J. 1995. Light-microscopic distribution and parasagittal organisation of muscarinic receptors in rabbit cerebellar cortex. J Chem Neuroanat 9(4):241-259.

Jaarsma D, Ruigrok TJ, Caffe R, Cozzari C, Levey AI, Mugnaini E, Voogd J. 1997. Cholinergic innervation and receptors in the cerebellum. Prog Brain Res 114:67-96.

Jakab RL, Hamori J. 1988. Quantitative morphology and synaptology of cerebellar glomeruli in the rat. Anat Embryol (Berl) 179(1):81-88.

Jelitai M, Puggioni P, Ishikawa T, Rinaldi A, Duguid I. 2016. Dendritic excitation-inhibition balance shapes cerebellar output during motor behaviour. Nat Commun 7:13722.

Kuijpers M, van Dis V, Haasdijk ED, Harterink M, Vocking K, Post JA, Scheper W, Hoogenraad CC, Jaarsma D. 2013. Amyotrophic lateral sclerosis (ALS)-associated VAPB-P56S inclusions represent an ER quality control compartment. Acta Neuropathol Commun 1:24.

Langer T, Fuchs AF, Scudder CA, Chubb MC. 1985. Afferents to the flocculus of the cerebellum in the rhesus macaque as revealed by retrograde transport of horseradish peroxidase. J Comp Neurol 235(1):1-25.

Langer TP. 1985. Basal interstitial nucleus of the cerebellum: cerebellar nucleus related to the flocculus. J Comp Neurol 235(1):38-47.

Lein ES, Hawrylycz MJ, Ao N, Ayres M, Bensinger A, Bernard A, Boe AF, Boguski MS, Brockway KS, Byrnes EJ, Chen L, Chen L, Chen TM, Chin MC, Chong J, Crook BE, Czaplinska A, Dang CN, Datta S, Dee NR, Desaki AL, Desta T, Diep E, Dolbeare TA, Donelan MJ, Dong HW, Dougherty JG, Duncan BJ, Ebbert AJ, Eichele G, Estin LK, Faber C, Facer BA, Fields R, Fischer SR, Fliss TP, Frensley C, Gates SN, Glattfelder KJ, Halverson KR, Hart MR, Hohmann JG, Howell MP, Jeung DP, Johnson RA, Karr PT, Kawal R, Kidney JM, Knapik RH, Kuan CL, Lake JH, Laramee AR, Larsen KD, Lau C, Lemon TA, Liang AJ, Liu Y, Luong LT, Michaels J, Morgan JJ, Morgan RJ, Mortrud MT, Mosqueda NF, Ng LL, Ng R, Orta GJ, Overly CC, Pak TH, Parry SE, Pathak SD, Pearson OC, Puchalski RB, Riley ZL, Rockett HR, Rowland SA, Royall JJ, Ruiz MJ, Sarno NR, Schaffnit K, Shapovalova NV,

Sivisay T, Slaughterbeck CR, Smith SC, Smith KA, Smith BI, Sodt AJ, Stewart NN, Stumpf KR, Sunkin SM, Sutram M, Tam A, Teemer CD, Thaller C, Thompson CL, Varnam LR, Visel A, Whitlock RM, Wohnoutka PE, Wolkey CK, Wong VY, Wood M, Yaylaoglu MB, Young RC, Youngstrom BL, Yuan XF, Zhang B, Zwingman TA, Jones AR. 2007. Genome-wide atlas of gene expression in the adult mouse brain. Nature 445(7124):168-176.

Lisberger SG. 2009. Internal models of eye movement in the floccular complex of the monkey cerebellum. Neuroscience 162(3):763-776.

Mapelli L, Solinas S, D'Angelo E. 2014. Integration and regulation of glomerular inhibition in the cerebellar granular layer circuit. Frontiers in cellular neuroscience 8:55.

Nagao S, Kitamura T, Nakamura N, Hiramatsu T, Yamada J. 1997a. Differences of the primate flocculus and ventral paraflocculus in the mossy and climbing fiber input organization. J Comp Neurol 382(4):480-498.

Nagao S, Kitamura T, Nakamura N, Hiramatsu T, Yamada J. 1997b. Location of efferent terminals of the primate flocculus and ventral paraflocculus revealed by anterograde axonal transport methods. Neurosci Res 27(3):257-269.

Neki A, Ohishi H, Kaneko T, Shigemoto R, Nakanishi S, Mizuno N. 1996. Metabotropic glutamate receptors mGluR2 and mGluR5 are expressed in two non-overlapping populations of Golgi cells in the rat cerebellum. Neuroscience 75(3):815-826.

Ohishi H, Ogawa-Meguro R, Shigemoto R, Kaneko T, Nakanishi S, Mizuno N. 1994. Immunohistochemical localization of metabotropic glutamate receptors, mGluR2 and mGluR3, in rat cerebellar cortex. Neuron 13(1):55-66.

Palay SL, Chan-Palay VE. 1974. Cerebellar cortex: cytology and organization. Berlin: Springer Verlag.

Paxinos G, Franklin KBJ. 2001. The mouse brain in stereotaxic coordinates. London: Academic Press.

Pietrajtis K, Dieudonné S. 2013. Golgi Neurons. Handbook of the cerebellum and cerebellar disorders: Springer. p doi: 10.1007/1978-1094-1007-1333-1008_1034.

Powell K, Mathy A, Duguid I, Hausser M. 2015. Synaptic representation of locomotion in single cerebellar granule cells. Elife 4.

Rancz EA, Ishikawa T, Duguid I, Chadderton P, Mahon S, Hausser M. 2007. High-fidelity transmission of sensory information by single cerebellar mossy fibre boutons. Nature 450(7173):1245-1248.

Ruigrok TJ. 2003. Collateralization of climbing and mossy fibers projecting to the nodulus and flocculus of the rat cerebellum. J Comp Neurol 466(2):278-298.

Ruigrok TJ, Hensbroek RA, Simpson JI. 2011. Spontaneous activity signatures of morphologically identified interneurons in the vestibulocerebellum. J Neurosci 31(2):712-724.

Ruigrok TJ, Osse RJ, Voogd J. 1992. Organization of inferior olivary projections to the flocculus and ventral paraflocculus of the rat cerebellum. J Comp Neurol 316(2):129-150.

Schonewille M, Luo C, Ruigrok TJ, Voogd J, Schmolesky MT, Rutteman M, Hoebeek FE, De Jeu MT, De Zeeuw CI. 2006. Zonal organization of the mouse flocculus: physiology, input, and output. J Comp Neurol 497(4):670-682.

Sekerkova G, Watanabe M, Martina M, Mugnaini E. 2014. Differential distribution of phospholipase C beta isoforms and diaglycerol kinase-beta in rodents cerebella corroborates the division of unipolar brush cells into two major subtypes. Brain Struct Funct 219(2):719-749.

Siegers JY, Short KR, Leijten LM, de Graaf M, Spronken MI, Schrauwen EJ, Marshall N, Lowen AC, Gabriel G, Osterhaus AD, Kuiken T, van Riel D. 2014. Novel avian-origin influenza A (H7N9) virus attachment to the respiratory tract of five animal models. J Virol 88(8):4595-4599.

Simat M, Parpan F, Fritschy JM. 2007. Heterogeneity of glycinergic and gabaergic interneurons in the granule cell layer of mouse cerebellum. J Comp Neurol 500(1):71-83.

Singec I, Knoth R, Ditter M, Frotscher M, Volk B. 2003. Neurogranin expression by cerebellar neurons in rodents and non-human primates. J Comp Neurol 459(3):278-289.

Singec I, Knoth R, Ditter M, Volk B, Frotscher M. 2004. Neurogranin is expressed by principal cells but not interneurons in the rodent and monkey neocortex and hippocampus. J Comp Neurol 479(1):30-42.

Sudhakar SK, Hong S, Raikov I, Publio R, Lang C, Close T, Guo D, Negrello M, De Schutter E. 2017. Spatiotemporal network coding of physiological mossy fiber inputs by the cerebellar granular layer. PLoS Comput Biol 13(9):e1005754.

Takikawa Y, Kawagoe R, Miyashita N, Hikosaka O. 1998. Presaccadic omnidirectional burst activity in the basal interstitial nucleus in the monkey cerebellum. Exp Brain Res 121(4):442-450.

Tan J, Epema AH, Voogd J. 1995. Zonal organization of the flocculovestibular nucleus projection in the rabbit: a combined axonal tracing and acetylcholinesterase histochemical study. J Comp Neurol 356(1):51-71.

Valera AM, Binda F, Pawlowski SA, Dupont JL, Casella JF, Rothstein JD, Poulain B, Isope P. 2016. Stereotyped spatial patterns of functional synaptic connectivity in the cerebellar cortex. Elife 5.

van Dorp S, De Zeeuw CI. 2015. Forward Signaling by Unipolar Brush Cells in the Mouse Cerebellum. Cerebellum (London, England).

van Riel D, Leijten LM, Kochs G, Osterhaus AD, Kuiken T. 2013. Decrease of virus receptors during highly pathogenic H5N1 virus infection in humans and other mammals. Am J Pathol 183(5):1382-1389.

Voges K, Wu B, Post L, Schonewille M, De Zeeuw CI. 2017. Mechanisms underlying vestibulo-cerebellar motor learning in mice depend on movement direction. J Physiol 595(15):5301-5326.

Vong L, Ye C, Yang Z, Choi B, Chua S, Jr., Lowell BB. 2011. Leptin action on GABAergic neurons prevents obesity and reduces inhibitory tone to POMC neurons. Neuron 71(1):142-154.

Voogd J, Glickstein M. 1998. The anatomy of the cerebellum. Trends Neurosci 21(9):370-375.

Voogd J, Schraa-Tam CK, van der Geest JN, De Zeeuw CI. 2012. Visuomotor cerebellum in human and nonhuman primates. Cerebellum (London, England) 11(2):392-410.

Wang Q, Henry AM, Harris JA, Oh SW, Joines KM, Nyhus J, Hirokawa KE, Dee N, Mortrud M, Parry S, Ouellette B, Caldejon S, Bernard A, Jones AR, Zeng H, Hohmann JG. 2014. Systematic comparison of adeno-associated virus and biotinylated dextran amine reveals equivalent sensitivity between tracers and novel projection targets in the mouse brain. J Comp Neurol 522(9):1989-2012.

Watanabe D, Inokawa H, Hashimoto K, Suzuki N, Kano M, Shigemoto R, Hirano T, Toyama K, Kaneko S, Yokoi M, Moriyoshi K, Suzuki M, Kobayashi K, Nagatsu T, Kreitman RJ, Pastan I, Nakanishi S. 1998. Ablation of cerebellar Golgi cells disrupts synaptic integration involving GABA inhibition and NMDA receptor activation in motor coordination. Cell 95(1):17-27.

Witter L, De Zeeuw CI. 2015. Regional functionality of the cerebellum. Curr Opin Neurobiol 33:150-155.

Zampini V, Liu JK, Diana MA, Maldonado PP, Brunel N, Dieudonne S. 2016. Mechanisms and functional roles of glutamatergic synapse diversity in a cerebellar circuit. Elife 5.

Zeilhofer HU, Studler B, Arabadzisz D, Schweizer C, Ahmadi S, Layh B, Bosl MR, Fritschy JM. 2005. Glycinergic neurons expressing enhanced green fluorescent protein in bacterial artificial chromosome transgenic mice. J Comp Neurol 482(2):123-141.

Zhang MD, Barde S, Szodorai E, Josephson A, Mitsios N, Watanabe M, Attems J, Lubec G, Kovacs GG, Uhlen M, Mulder J, Harkany T, Hokfelt T. 2016. Comparative anatomical distribution of neuronal calcium-binding protein (NECAB) 1 and -2 in rodent and human spinal cord. Brain Struct Funct 221(7):3803-3823.

Zhou H, Lin Z, Voges K, Ju C, Gao Z, Bosman LW, Ruigrok TJ, Hoebeek FE, De Zeeuw CI, Schonewille M. 2014. Cerebellar modules operate at different frequencies. Elife 3:e02536.

Figure legends

Figure 1. Choline Acetyltransferase (ChAT) immunostaining outlines the basal interstitial nucleus (BIN) in macaque cerebellum

a-e: Low-power (a) and high power (b-e) photomicrographs of ChAT immunoperoxidase diaminobenzidine (DAB) stained coronal sections of Macaque cerebellum illustrating intensely stained BIN neurons in the basal white matter between the flocculus and the cerebellar nuclei (a,b), and ChAT+ beaded fibers in the floccular granule cell layer (a,d). The photomicrograph in c illustrates that ChAT+ BIN neurons (arrow) are considerably larger than ChAT+ neurons in group Y (arrow head). No or minimal ChAT+ fibers occur in the dorsal paraflocculus (DPFl; a,e). Sections are counterstained with thionin (blue).

f: Plots of ChAT+ BIN neurons (red dots) and relative density of ChAT+ beaded fibers (violet staining) in serial coronal macaque cerebellar sections. Cerebellar and vestibular nuclei are indicated in light blue and green, respectively.

Abbreviations: DCo, dorsal cochlear nucleus; DPFl, Dorsal paraflocculus; Fl, Flocculus; icp, inferior cerebellar peduncle; IntA, anterior interposed cerebellar nucleus; IntP, posterior interposed nucleus; Lat, lateral cerebellar nucleus; mcp, middle cerebellar peduncle; LVe, lateral vestibular nucleus; MVe, medial vestibular nucleus; Nod, Nodulus; Pr, prepositus hypoglossi; SpVe, spinal vestibular nucleus; SuVe, Superior vestibular nucleus.

Scale bars: a, 500 µm; c, 200 µm; b and e, 50 µm

Figure 2. Macaque BIN neurons provide GABAergic input to the granule cell layer of the flocculus

a-e: Double labelling confocal immunofluorescence for ChAT and glutamic acid decarboxylase 65/67 (GAD) shows that ChAT+ neurons in the BIN (a,b) and ChAT+ axonal terminals in the granule cell layer of the flocculus (arrows in c) are also positive for GAD, while ChAT+ mossy fibers in the granule cell layer of the nodulus are negative for GAD (arrow in d). Note in panel a and b, that the BIN also contains ChAT-GAD+ neurons (arrow heads in a, b). Also note that both ChAT+ and ChAT- BIN neurons are only sparsely covered by GAD+ nerve terminals (thin arrow in b'''), which differs from deep cerebellar nuclear neurons whose cell bodies and proximal dendrites are densely innervated by GAD+ synaptic terminals (e). Note in c' that ChAT+GAD+ boutons (arrows) complement ChAT-GAD+ boutons (arrow heads) in the same glomerulus.

f, g: ChAT/mGluR2 double staining (f) and ChAT/mGluR2/VIAAT triple staining (g), shows that ChAT+ fibers and boutons (arrows in f and g) are always mGluR2-, and complement mGluR2+ boutons (arrow heads in f and g) in glomeruli in the floccular granule cell layer. Both ChAT+ and

mGluR2+ boutons stain positive for VIAAT. In g, also note the presence of ChAT-mGluR2-VIAAT+ nerve terminals (double-headed arrow).

h: Serial confocal optical sections and 3D-reconstructions of an exemplary mossy fiber ending labeled by VGluT1 that is surrounded by ChAT+VIAAT+ and ChAT-VIAAT+ nerve endings.

i, j: High magnifications of ChAT/calretinin (CR) double staining in the granule cell layer of the ventral paraflocculus showing examples of CR+ UBCs with a substantial number of ChAT+ nerve endings surrounding their brush-like dendritic arbor (arrows in i) as well as CR+ UBCs with virtually no ChAT+ nerve endings surrounding the 'brush' (arrow heads in j).

Scale bars: a, 100 µm; b-f, 25 µm; g, 10 µm; h, 5 µm; i, 20 µm.

Figure 3. ChAT-staining outlines the BIN in human cerebellum

a: Low- and high-power (inserts) photomicrographs of ChAT immunoperoxidase diaminobenzidine (DAB) stained coronal sections of human cerebellum showing a cluster of ChAT stained neurons in the white matter between the flocculus and the lateral cerebellar nucleus (Lat) that is reminiscent of the BIN in macaque.

b: Plots of ChAT+ neurons in the basal white matter of human cerebellum. ChAT+ neurons are most abundant in the white matter, extending from the ventrolateral aspect of the lateral cerebellar nucleus (Lat) to the peduncles of the flocculus and the accessory paraflocculus (APFl).

c, d: GAD immunoperoxidase-DAB (c) and immunofluorescent (d) staining of BIN neurons arrows in c and d. The BIN neuron shown in d (arrow) also is ChAT+.

e-h: ChAT immunoperoxidase-DAB staining reveals variable densities of ChAT+ beaded fibers in the granule cell layer of different lobules that correlate with the presence of ChAT+ Golgi cells: in the flocculus, high densities of ChAT+ fibers occurs in parts of the granule cell layer containing ChAT+ Golgi cells (white arrows in f, g), while moderate levels of ChAT+ fibers occur in parts without ChAT+ Golgi cells (e). Moderate levels of ChAT+ fibers also occur in lobules with ChAT+ Golgi cells, e.g. lobule 8 of the vermis (g). Lobules of the hemispheres with no ChAT+ Golgi cells do not show ChAT+ fibers (h, biventral lobule).

Scale bars: a, 1 mm (overview) and 100 µm (insert); c and h, 100 µm (also for e-g); d, 20 µm.

Figure 4. BIN neurons in rat

a-c: Plot (a) and photomicrographs (b, c) of retrogradely cholera toxin ß subunit (CTB) labeled BIN neurons (red dots in a; red arrows in c) following a small CTB injection in the flocculus (purple area in a); sections and plots are from rat 836 described in (Ruigrok, 2003). Note that retrogradely CTB labeled neurons also occur in the vestibular nuclei (blue dots in a). Arrowheads in c point to unlabeled BIN neurons.

d: Double labelling confocal immunofluorescence for GAD and CTB shows that retrogradely CTB labeled BIN neurons (arrows) are GAD+.

e: Double labelling confocal immunofluorescence for GAD and NeuN shows that GAD+ BIN neurons in the rat floccular white matter (arrows) are NeuN+.
Scale bars: b,d and e 100 µm; c, 50 µm.

Figure 5. Evoked action potentials and spontaneous EPSC in rat BIN neurons

a-d: Example of a recorded BIN neuron filled with 1% neurobiotin (NB) visualized with A488-streptavidin. NB filling reveals an extensive axonal tree, and dendritic branches that may extend in the granule cell layer. Axonal branches are mGluR2- and contact multiple glomeruli characterized by the presence of VGluT1+ mossy fiber endings and mGluR2+ Golgi cell axons (c, d).
Scale bars: b, 100 µm; c, 25 µm; d, 10 µm.
e: Example traces of subthreshold depolarization of and evoked action potentials with increasing depolarizing current injection.
f: Average firing rate of BIN neurons (mean ± SE, n=7 cells) as a function of the injected current during the depolarizing step.
g: Action potential threshold and amplitudes (individual values and means ±SE).
h-j: Example traces (h), cumulative distribution of sEPSC activity from an exemplary BIN neuron (i), and mean ± SE of sEPSC frequencies and amplitudes (j) of recorded BIN neurons (n=6).

Figure 6. BIN neurons in mouse flocculus identified by retrograde CTB tracing and Necab1 immunostaining

a, b: Double labelling confocal immunofluorescent image (a) and plot (b) of CTB-labeled BIN neurons (arrows in a; red dots in b) following CTB injection in the flocculus (purple area in b outline the injection area) of GlyT2GFP transgenic mice (a is from mouse Gly1; b is from mouse Gly4). All retrogradely CTB labeled BIN neurons are also positive for GFP (arrows in a). GlyT2-GFP+ BIN neurons that are not positive for CTB are indicated by green dots in b.
c, d: Confocal immunofluorescence of mGluR2 (c) and muscarinic M2 receptor (d) in the flocculus of a GlyT2GFP transgenic mouse. GlyT2+ Golgi cells in the granule cell layer (gl) stain positive for mGluR2 (arrow heads in c) and muscarinic M2 receptor (arrow heads in d), while GlyT2GFP BIN neurons are M2+ and mGluR2- (small arrows in c and d). wm, white matter
e: *In situ hybridization* image from Allan Brain Atlas showing that mGluR2 (*Gm2*) mRNA is expressed in granule cell layer (gl) but not in white matter cells of the flocculus, while muscarinic M2 receptor (*Chrm2*), GAD65 (*Gad2*), AChE and Lgi2 mRNA occur cells in both the granule cell layer and the white matter (red arrows). Necab1 mRNA, instead, is expressed in cells in the floccular white matter, but not in the granule cell layer.

f, g: Confocal images of Necab1 immunostaining in the flocculus of a GlyT2GFP mouse (f), and a non-trangenic mouse receiving a CTB tracer injection in the flocculus (g). Intense Necab1 staining is present in GlyT2GFP+ neurons (yellow arrows in f) and CTB-traced BIN neurons (g, see inserts). Note in f', that dendrites of some Necab1+ BIN neurons may extend in the granule cell layer (white arrows in f'). Also note in f, a population of Necab1+ neurons in the granule cell layer of the paraflocculus (cyan arrow head in f"), while no Necab1+ neurons occur in the granule cell layer of the flocculus (yellow arrow head in f' points to a GlyT2GFP+ Golgi cell in the flocculus).
Scale bars: a,f and g, 100 µm; d, 10 µm.

Figure 7. Absence of Necab1+ and Neurogranin+ Golgi cells in mouse flocculus

a,b: Confocal images of neurogranin-immunostaining in GlyT2GFP mouse cerebellar cortex, showing that in lobule 4-5 of the vermis (a) neurogranin (NG, rabbit antibody) labelling occurs in GFP- (white arrow head) and GFP+ Golgi cells (yellow arrow head), while in the flocculus (Fl in b) there are no neurogranin+ Golgi cells. Note in flocculus, that BIN neurons (white arrow in b') do not stain for neurogranin, while sporadic neurogranin+ cells can be observed in the adjacent ventral paraflocculus (PFl, yellow arrow head in insert in b).

c: Staining for neurogranin (mouse antibody) and Necab1 in vermis 4-5 of GlyT2GFP mouse illustrates that neurogranin and Necab1coditribute in GFP- Golgi cells (white arrow heads), and show variable codistribution in GFP+ Golgi cells (e.g. yellow arrow head points to GlyT+neurogranin+Necab1+ cell).

d: Staining for neurogranin (rabbit antibody) and Lgi2 in vermis 4-5 of GlyT2GFP mice shows that Lgi2 is present in neurogranin+GFP- (white arrow heads), neurogranin+GFP+ (yellow arrow heads), and neurogranin-GFP+ Golgi cells (yellow arrow).

e: Plot of vermis 4-5 in coronal section of GlyT2GFP mouse stained for Lgi2 and neurogranin; the plot outlines the distribution of type 1-3 Golgi cells (blue dots, Lgi2+GFP+), type 4 Golgi cells (light brown squares, Lgi2+GFP-NG+) and Lugaro/globular cells (green dots, Lgi2+GFP-NG-). Lgi2+GFP- cells always were also positive for neurogranin.

f,g: Confocal image (f) and plot (g) illustrating the distribution of Golgi cells (Lgi2+GFP+Necab1-, yellow arrow heads in f, blue dots in g), Lugaro/globular cells (green dots, Lgi2+GFP-Necab1-), and BIN neurons (magenta dots, Lgi2+GFP+Necab1+) in coronal sections of the flocculus.
Scale bars: a, 100 µm; b, 200 µm; c, d, f, 50 µm.

Figure 8. BIN neurons innervate granule cell dendrites in glomeruli in mouse flocculus

a-c: Injection of AAV2-CAG-eGFP virus in the white matter and the hilus of the flocculus (a,b) results in labelling of BIN neurons and their axons in the floccular granule cell layer (b,c). Co-immunostaining for VIAAT shows that GFP+ axons display VIAAT+ varicosities (white boutons, e.g.

yellow arrow heads in c). Double-labeled GFP+VIAAT+ varicosities are intermingled with GFP-VIAAT+ boutons (magenta boutons, cyan arrow heads in c).

d-f: Transmission electron microscopy of anti-GFP immunoperoxidase-DAB precipitate in the floccular granule cell layer following AAV2-CAG-eGFP infection of BIN neurons. DAB precipitate is associated with presynaptic boutons (outlined by green color coding) that form synapses (red arrows in d) with granule cell dendrites (Grd, blue color coding). Post-embedding anti-GABA immunogold-labeling shows that DAB+ axon terminals are also enriched in GABA (e, f). Mossy fiber endings and putative Golgi cell axons are coded in yellow and red, respectively.

g,h: Series of optical sections (g) and 3-dimensional reconstruction (h) of a glomerulus innervated by GFP-labeled BIN axons and labeled for mGluR2, VIAAT and VGluT1. Note that the VGluT1+ mossy fiber rosette is surrounded by GFP+mGluR2-VIAAT+ (small arrows), GFP-mGluR2+VIAAT+ (arrow heads) and single-labeled GFP-mGluR2-VIAAT+ boutons (double-headed arrow).

i: Bar graph showing the area of VIAAT+ nerve endings in floccular granule cell layer that co-distribute with GFP labeled BIN axon endings (green bars) or mGluR2 staining (red bars). Analyzed sections are from 3 mice with AAV2-CAG-GFP virus injections in the BIN showing the highest amount of BIN axonal labeling in the flocculus (mouseV2, mouseV3, mouseV5; see material and methods for details).

j,k: Exemplary confocal images (j) and graph (k) showing that in the anterior vermis more than 90% of the VIAAT+ axon endings is mGluR2+, whereas in the flocculus the proportion is 60%, as illustrated by the large proportion of single labeled VIAAT+ terminals (green boutons in upper panel in j).

l: Cartoon illustrating how BIN axon terminals may complement mGluR2+ Golgi axon terminals in floccular glomeruli.

Scale bars: b, 250 µm; c, 5 µm; d -f, 500 nm; g, 2 µm; j, 50 µm.

Figure 9. BIN neurons are innervated by VGluT2+ axons arising in the medial medullary reticular formation

a: Confocal image of NeuN/VGluT1/VGluT2 triple staining in rat flocculus showing that cell body and proximal dendrites of BIN neurons are covered by VGluT2+ axon terminals.

b-d: Representative images of injection spot (b) and anterogradely-labeled fibers in the floccular white matter (c), and map of injection area's of selected BDA (biotinylated dextran amine) anterograde tracing experiments (d) showing that injections targeting the gigantocellular reticular nucleus (Gi) in the rostral medullary reticular formation result in labelling of fibers contacting BIN neurons. Injections in surrounding areas (indicated in red) did not result in labeling of fibers innervating BIN neurons, but to variable extend produced labeling of mossy fibers innervating floccular granule cell layer.

e: Maximal projection (left panel, total thickness = 12 µm) and single optical section (middle and right panel, z = 1 µm) illustrating a BDA-labeled fiber from the Gi innervating a BIN neuron (labeled with

anti-muscarinic M2 receptor antibody). Arrows in maximal projection and single optical section point to the same nerve endings. Co-staining for VGluT2+ shows that nerve endings from labeled fibers are VGluT2+, and that this cell is innervated by additional VGluT2+ nerve endings from non-labeled fibers (arrow heads).

f: Maximal projections of exemplary BIN neurons identified by (Necab1-immunostaining) innervated by GFP+-beaded fibers following AAV-floxed-GFP injection in the Gi of VGluT2-Cre mouse.

g: Immunoperoxidase-DAB staining of retrogradely labeled medium-sized neurons (arrows in G') in the Gi following CTB injection in hilus of the flocculus. Note that the large Gi neurons (arrow heads) are not labeled for CTB.

h: Schematic representation of BIN neurons and glutamatergic BIN afferent fibers (baf) from the Gi in the floccular circuitry.

Scale bars: a and f', 20 µm; b and g, 500 µm; c, 100 µm; d and g'', 10 µm; g', 50 µm.

Figure 10. BIN neurons in rabbit

a, b: Low- (a) and high-magnification photomicrographs (a', b) illustrating retrogradely-labeled neurons in the white matter between the medial cerebellar peduncle (mcp) and the anterior vermis (arrows in a', b) following WGA-HRP injection in the rabbit flocculus (a). Images are from experimental animals (K244 and K227) from previously reported experiments (Tan et al., 1995).

c, d: GAD-immunoperoxidase staining reveals GAD+ neurons in the white matter medio-caudal of the mcp, while a few GAD+ neurons are present in the floccular white matter lateral of the mcp. In the plot in d, all GAD+ cells in white areas surrounding the mcp are plotted. The distribution and size of GAD+ neurons corresponded to the distribution of WGA-HRP tracing experiments.

Scale bars: a and c, 500 µm; a', 50 µm; b and c'', 20 µm; c', 200µm.

Figure 11. BIN neurons in ferret

Low-(a) and high-magnification (a') images and plots (b) of GAD-immunostaining in ferret flocculus illustrating a cluster of GAD+ neurons (red arrows in a', red dots in b) in the white matter facing the transition zone between the flocculus and the ventral paraflocculus.

Scale Bar: a, 500 µm.

Table 1: reagents and resources

Antibody (concentration)	**Immunogen**	**Source, catalog #, RRID**
Ms anti-calbindin (1:10000)	Bovine kidney calbindin-D	Sigma, C8666; RRID:AB_2313712
Rabbit anti-calbindin (1:10000)	Recombinant rat calbindin D-28k	Swant, CB38; RRID:AB_10000340
Rabbit anti-calretinin (1:5000)	Recombinant human calretinin-22k	Swant, 6B3; RRID:AB_10000320
Goat anti-CTB (1:5000)	Purified cholera toxin B subunit	List Labs , #703; RRID:AB_2313637
Goat anti-ChAT (1:500)	Purified ChAT from human placenta	Millipore, AB144P; RRID:AB_11214092
Rabbit anti-GABA (1:1000)	GABA conjugated to BSA	Sigma, A2052; RRID:AB_477652
Rabbit anti-GAD65/67 (1:2000)	rat GAD65 C-terminus (aa572-585)	Millipore, AB1511, RRID:AB_90715
Ms anti-GAD67, clone 1G10.2 (1:1000)	Recombinant GAD67 protein	Millipore, MAB5406; RRID:AB_2278725
Rabbit anti-GFP (1:5000)	Purified GFP from Aequorea Victoria	AbCam , #290; RRID:AB_303395
Rat anti-Lgi2 (1:10 culture supernatant)	Lgi2-Fc fusion protein	Dies Meijer, clone Lgi2-10D6
Ms anti-mGluR2 Clone mG2Na-s (1:2000)	GST-fusion protein containing aa87-134 of mouse mGluR2	AbCam, ab15672; RRID:AB_302021
Rat anti-muscarinic M2 receptor, clone M2-2-B3 (1:500)	GST-fusion protein containing i3 loop (aa225-359) of M2 receptor	Millipore, MAB367; RRID:AB_94952
Rabbit anti-Necab1 (1:1000)	Recombinant human Necab1 fragment (aa206-278)	Sigma, HPA023629; RRID:AB_1848014
Ms anti NeuN, clone A60 (1:4000)	Purified cell nuclei from mouse brain	Millipore, MAB377; RRID:AB2298772
Ms anti-Neurogranin, clone 898502 (1:100)	Recombinant human neurogranin	R&D systems, MAB7947
Rabbit anti-Neurogranin (1:2000)	Recombinant rat neurogranin	Millipore, AB5620; RRID:AB_91937
Guinea pig anti-VIAAT (1:1000)	Recombinant rat VIAAT fragment (aa2-115)	Synaptic Systems, 131004;RRID: AB_887873
Rabbit anti-VIAAT (1:1000)	Peptide corresponding to aa75-87 of rat VIAAT	Synaptic Systems, 131003;RRID: AB_887869
Guinea Pig anti-VGluT1 (1:4000)	Unspecified peptide from rat VGluT1	Millipore, AB5905;RRID: AB_2301751
Rabbit anti-VGluT1 (1:4000)	Recombinant rat VGluT1 fragment (aa456-560)	Synaptic Systems, 135 002,RRID: AB_2315546
Guinea pig anti-VGluT2 (1:2000)	KLH-conjugated peptide corresponding to rat VGluT2 C-terminus	Millipore, AB2251; RRID:AB_1587626
Ms anti-VGluT2 (1:1000)	Recombinant rat VGLUT2	Millipore, MAB5504; RRID:AB_2187552
Rabbit anti-VGluT2 (1:2000)	Recombinant rat VGluT2 fragment (aa510-582)	Synaptic systems, 135402; RRID: AB_2187539
Tracers	**Source**	**Catalog #, RRID**
Cholera toxin b-subunit (CTB), low salt	List Biological Labs	#104
biotin dextran amine 10 kDa (BDA-10000)	ThermoFisher	D1956; RRID:AB_2307337
AAV-vector	**Source**	**Catalog #**
AAV1.CAG.CI.eGFP.WPRE.rBG	Penn Vector Core	AV-1-PV1963
AAV1.CAG.Flex.eGFP.WPRE.bGH (AllenInstitute854)	Penn Vector Core	AV-1-ALL854
Mutant mouse models	**Source/reference**	**MGI number/Catalog #**
GlyT2-GFP	Zeilhofer et al., 1995	MGI:105090
VGluT2-ires-cre	Jackson Laboratories	JAX#016963

Table 2: number and molecular markers of BIN neurons in mammalian species examined in this study.

Species	**number of neurons (*10^3) $**	**markers**			
		GAD65/67	ChAT	Muscarinic M2	Necab1
Macaque	1.3 ± 0.2 (ChAT)	+	+/-	+	-
	2.2 ± 0.2 (GAD)				
Man	4.6 ± 0.7 (ChAT)	+	+/-	+	N.D.
Rat	0.66 ± 0.06 (GAD)	+	-	+	-
Mouse	0.33 ± 0.02 (GlyT2-GFP)	+	-	+	+
Rabbit	0.8 ± 0.2 (GAD)	+	-	+	N.D.
Ferret	1.1 ± 0.1 (GAD)	+	-	+	-

$ Numbers represent means ± S.E. per half cerebellum, and are extrapolated from counting 1 in 4 (mouse, rat), 1 in 5 (ferret) and 1 in 10 (rabbit, macaque, man) serial sections labeled for the marker in brackets. N.D., not determined

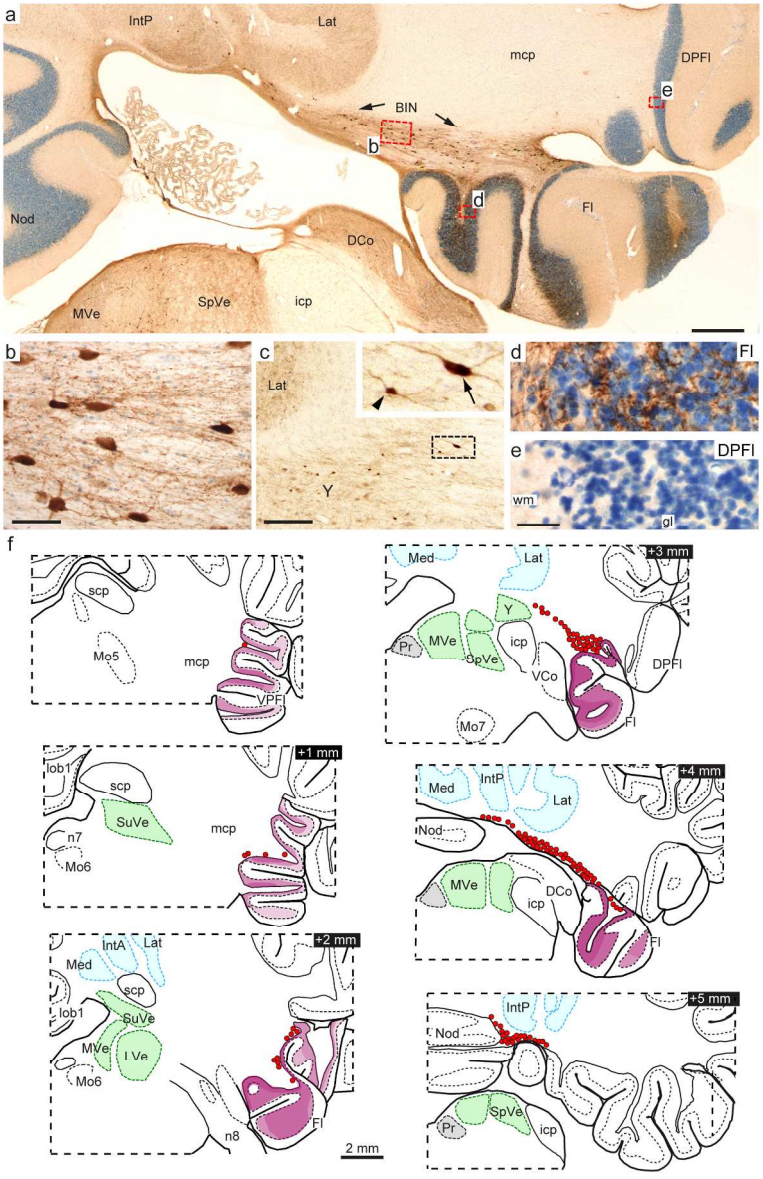

Figure 1. Choline Acetyltransferase (ChAT) immunostaining outlines the basal interstitial nucleus (BIN) in macaque cerebellum

166x253mm (300 x 300 DPI)

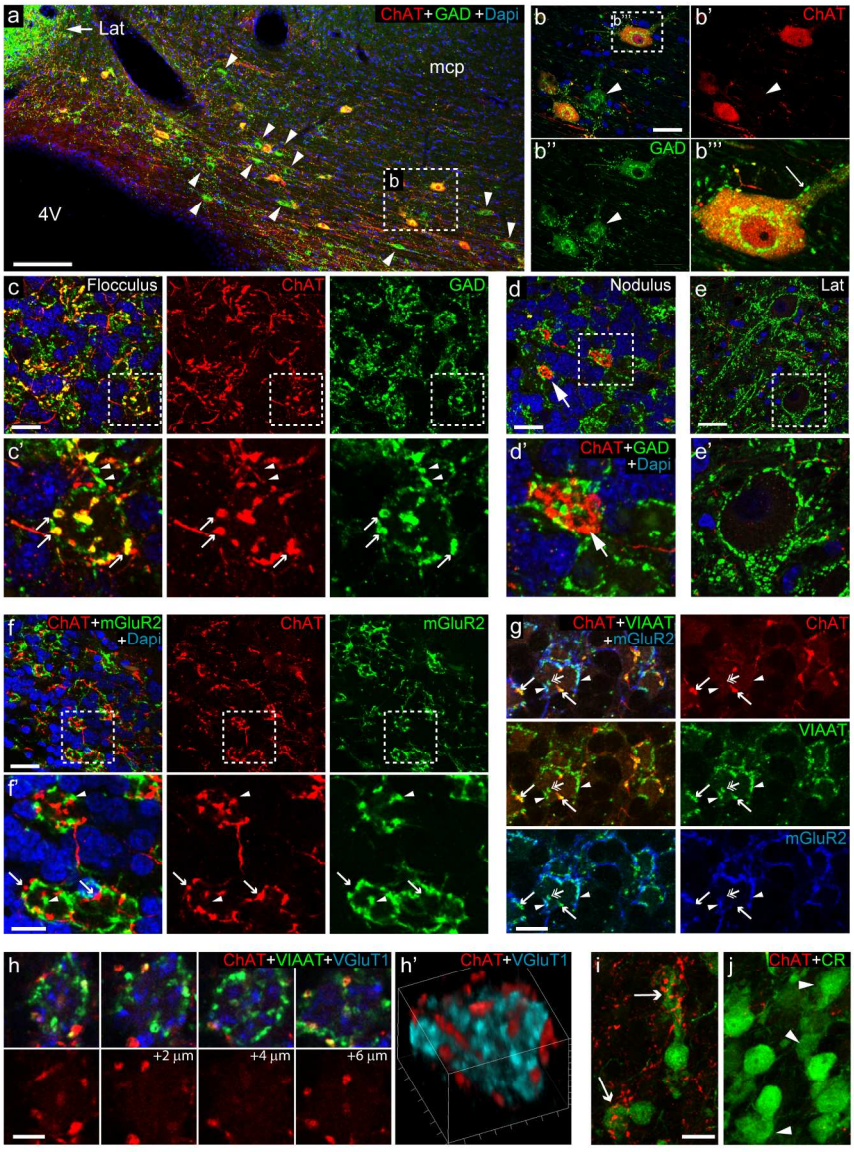

Figure 2. Macaque BIN neurons provide GABAergic input to the granule cell layer of the flocculus

169x227mm (300 x 300 DPI)

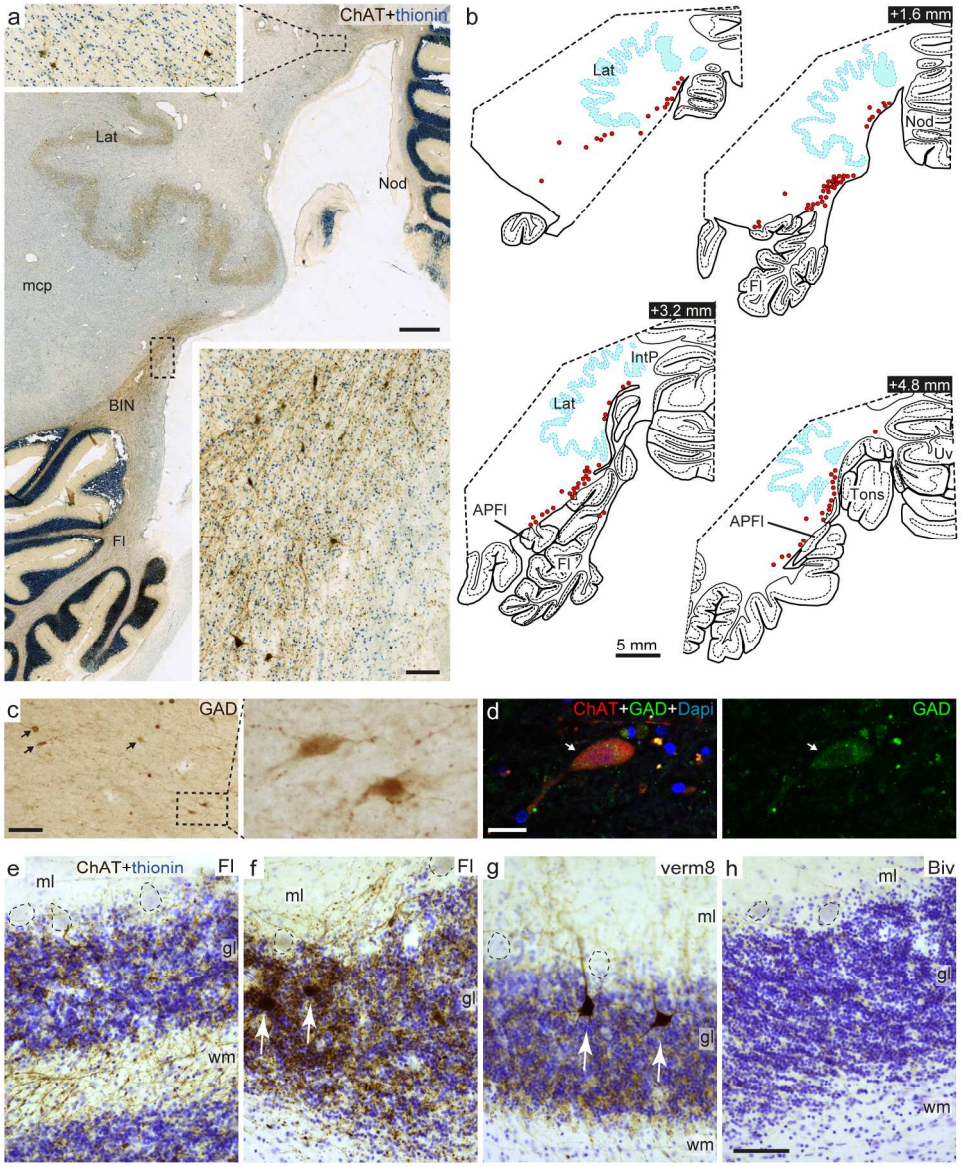

Figure 3. ChAT-staining outlines the BIN in human cerebellum

176x215mm (300 x 300 DPI)

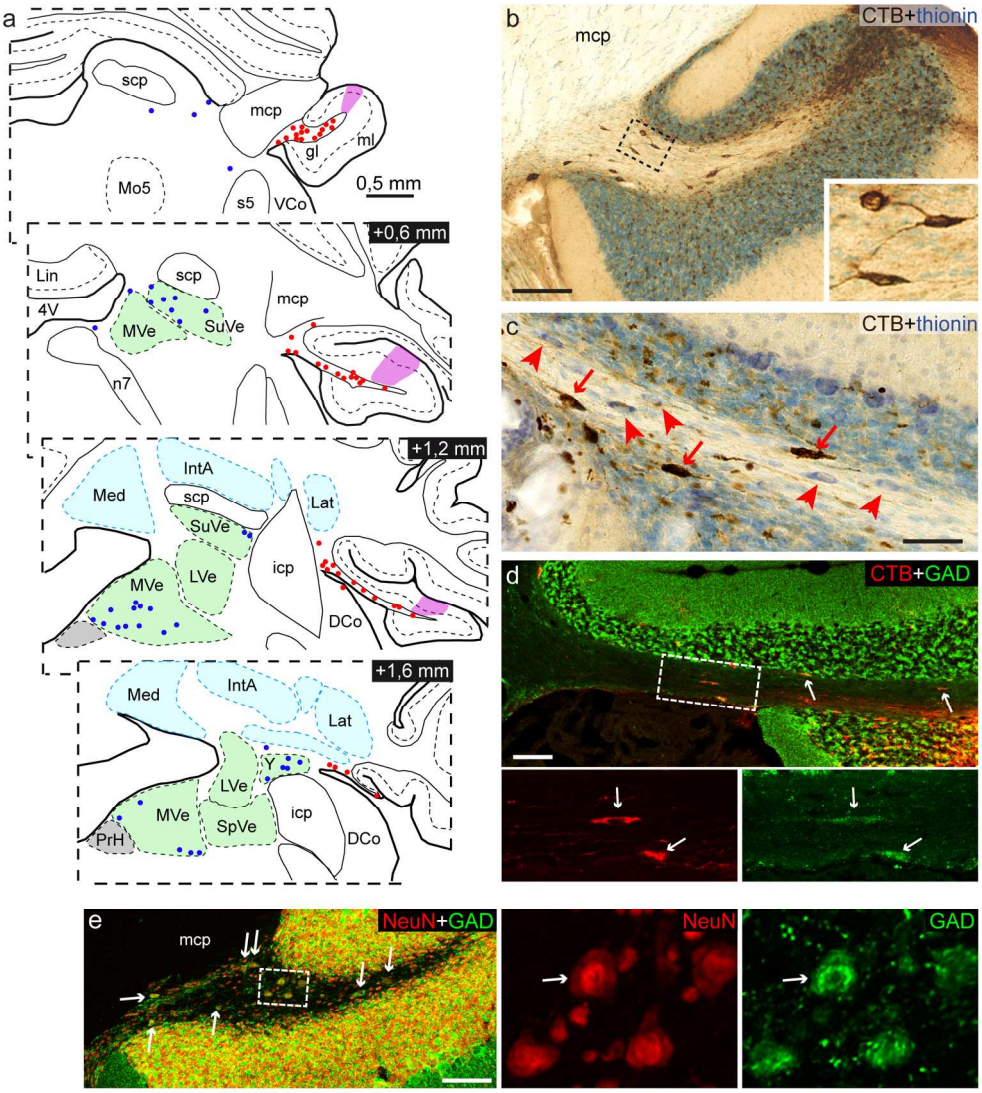

Figure 4. BIN neurons in rat

168x187mm (300 x 300 DPI)

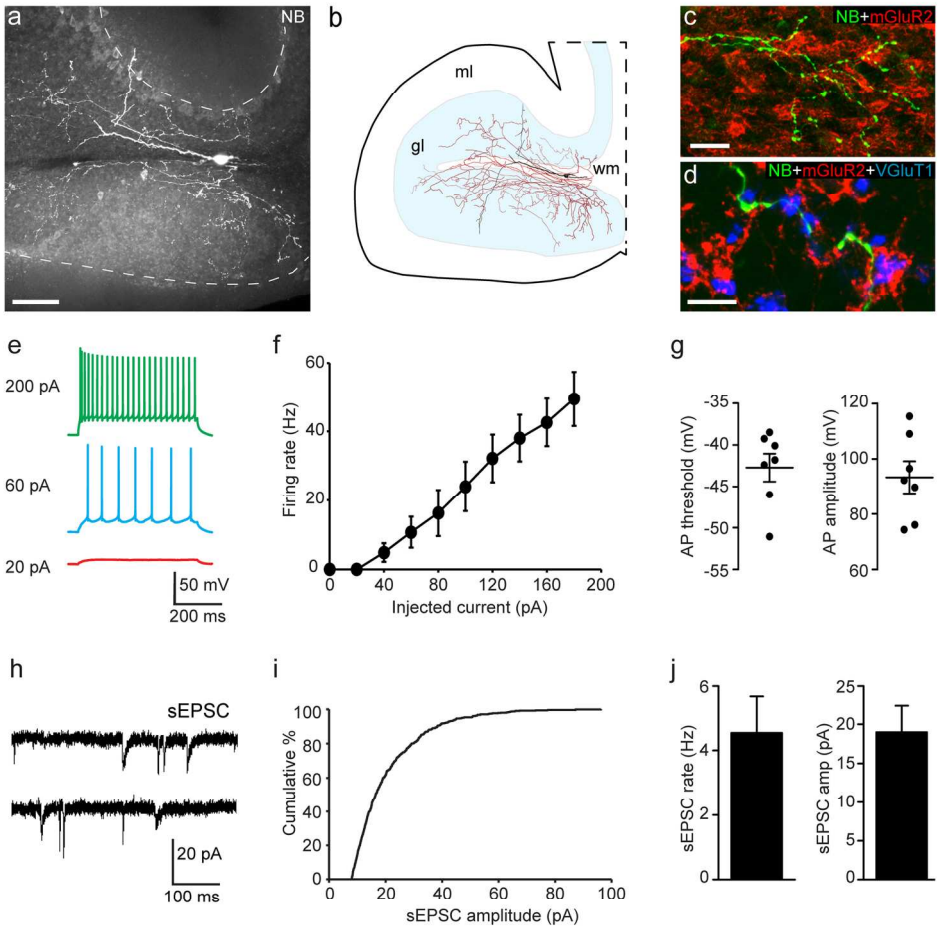

Figure 5. Evoked action potentials and spontaneous EPSC in rat BIN neurons

164x165mm (300 x 300 DPI)

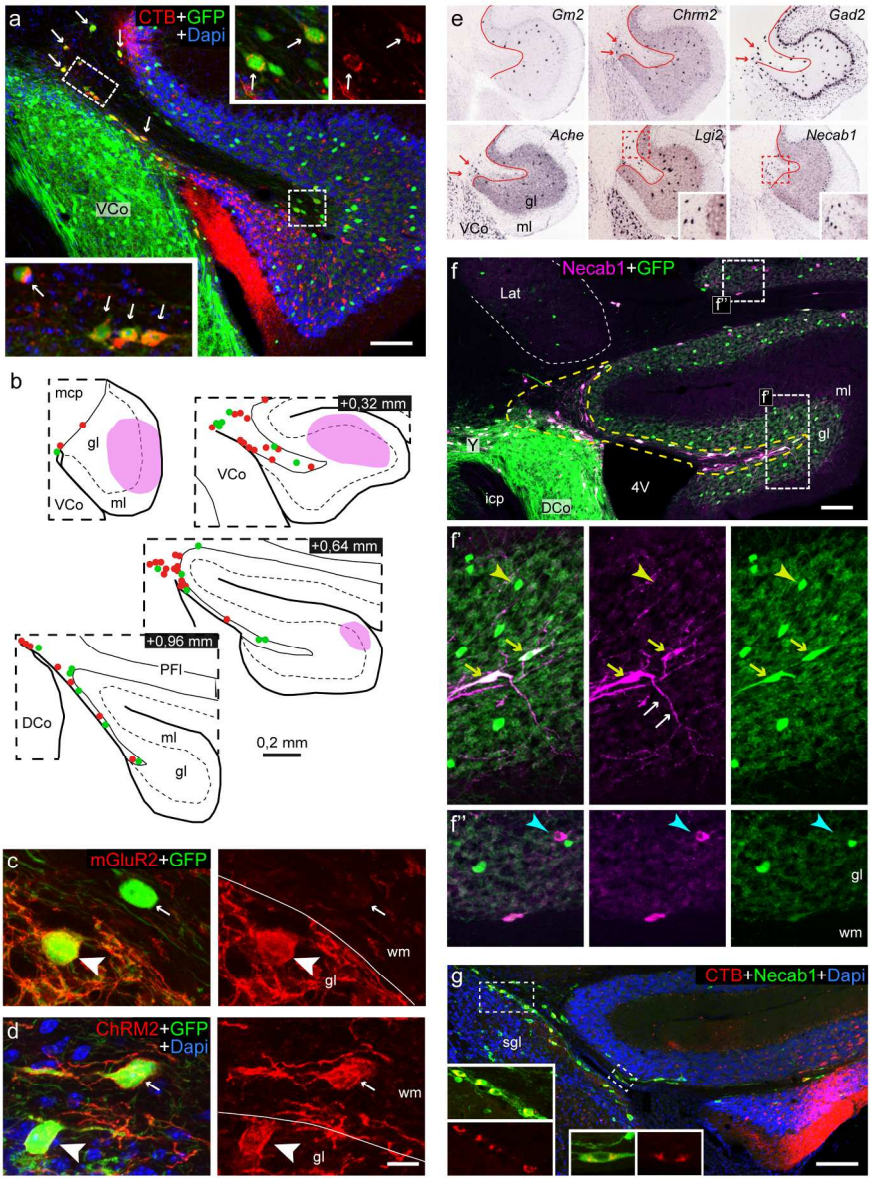

Figure 6. BIN neurons in mouse flocculus identified by retrograde CTB tracing and Necab1 immunostaining

171x228mm (300 x 300 DPI)

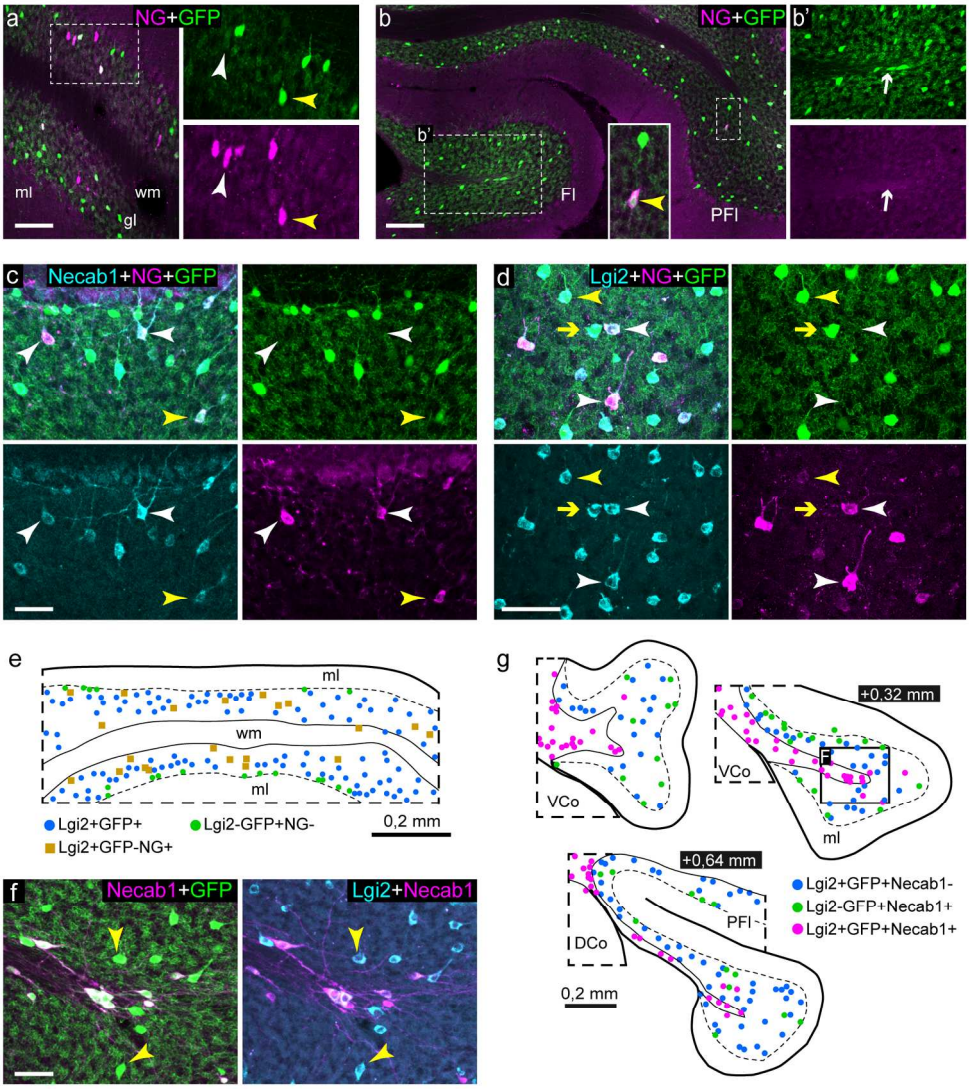

Figure 7. Absence of Necab1+ and Neurogranin+ Golgi cells in mouse flocculus

170x192mm (300 x 300 DPI)

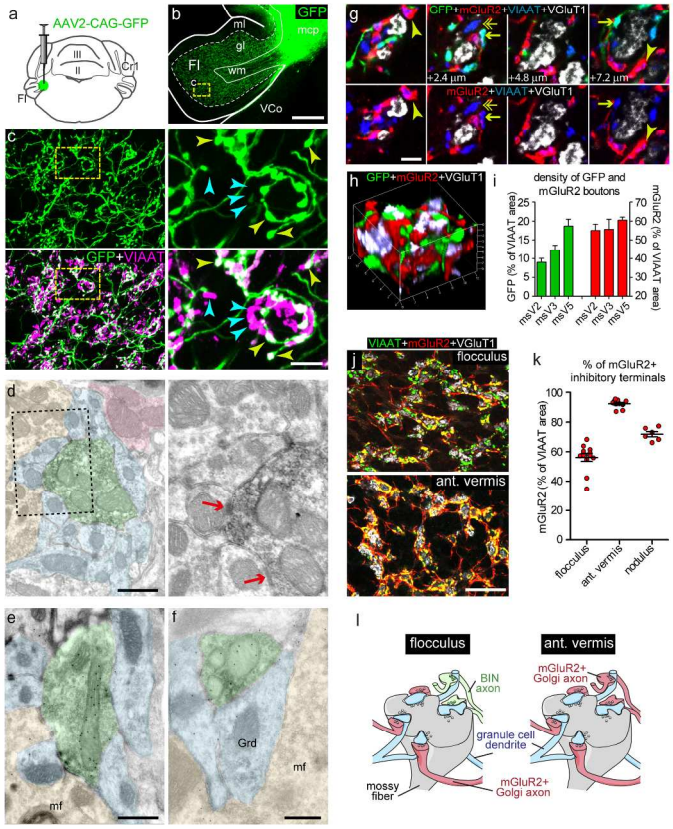

Figure 8. BIN neurons innervate granule cell dendrites in glomeruli in mouse flocculus

210x297mm (300 x 300 DPI)

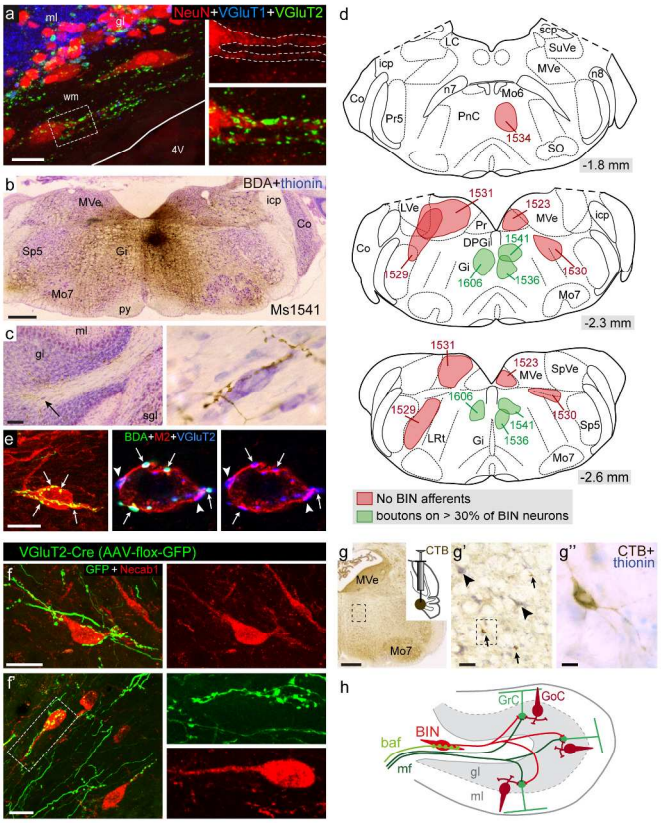

Figure 9. BIN neurons are innervated by VGluT2+ axons arising in the medial medullary reticular formation

210x297mm (300 x 300 DPI)

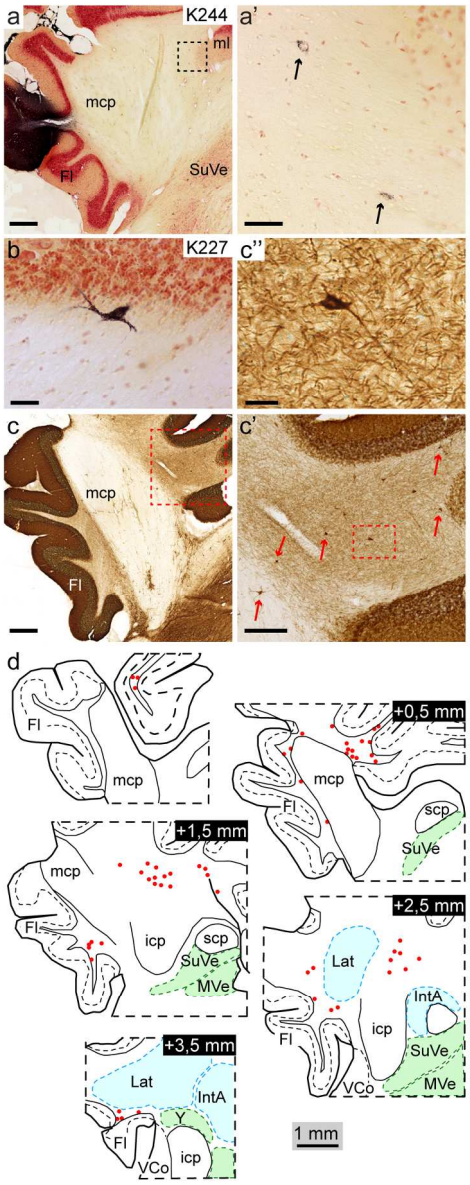

Figure 10. BIN neurons in rabbit

88x210mm (300 x 300 DPI)

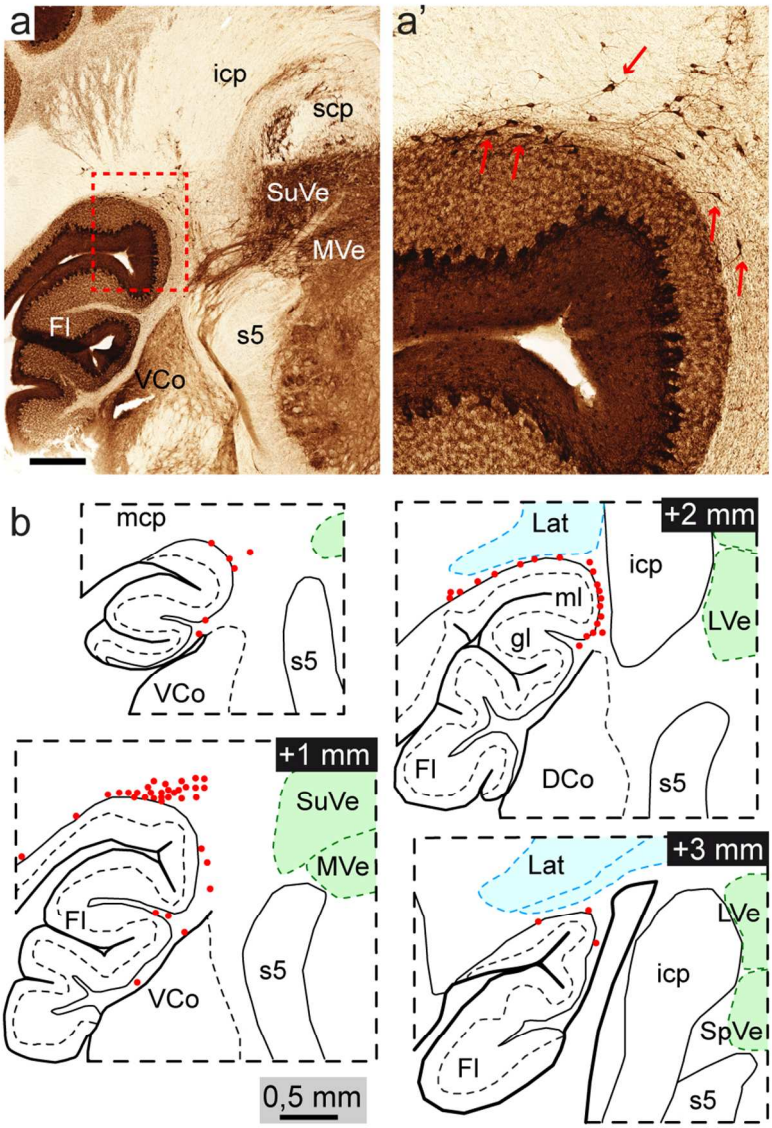

Figure 11. BIN neurons in ferret

89x127mm (300 x 300 DPI)